Polymer 285 (2023) 126311

Contents lists available at ScienceDirect

Polymer

journal homepage: www.elsevier.com/locate/polymer

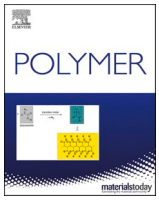

Poly (butylene succinate): Low-temperature nucleation and crystallization, complex morphology and absence of lamellar thickening

René Androsch [a,*], Katalee Jariyavidyanont [a], Andreas Janke [b], Christoph Schick [c,**]

[a] Interdisciplinary Center for Transfer-oriented Research in Natural Sciences (IWE TFN), Martin Luther University Halle-Wittenberg, 06099, Halle/Saale, Germany
[b] Leibniz-Institut für Polymerforschung Dresden e.V., Hohe Str. 6, 01069, Dresden, Germany
[c] Institute of Physics, University of Rostock, 18051, Rostock, Germany

ARTICLE INFO

Keywords:
Poly (butylene succinate) (PBS)
Crystallization
Crystal morphology
Secondary crystallization
Lamellar thickening
Crystal perfection
Rigid amorphous fraction

ABSTRACT

Melt-crystallization of poly (butylene succinate) (PBS) at largely different melt-supercooling was analyzed by X-ray scattering techniques, direct imaging using microscopy, and by fast scanning chip calorimetry, with the latter employed to achieve high melt-supercooling. Crystallization at 100 and 20 °C, representing structure formation at low and high melt-supercooling, respectively, yields lamellae with thicknesses of around 8 and 4 nm. In both cases, lamellar thickening is excluded as main mechanism of isothermal secondary crystallization, suggesting that absence of intracrystalline chain-sliding diffusion is not dependent on the absolute value of the thickness of lamellae. The wide-angle X-ray pattern of PBS crystallized at low temperature shows less and broader peaks than in case of PBS crystallized at high temperature, pointing to presence of crystal defects, and causing an enlargement of the unit cell. Secondary crystallization leads to an increase of the melting temperature, being distinctly larger (per unit annealing time) for low-temperature crystallized PBS. Since lamellar thickening is absent, and imperfection of the bulk crystal structure persists even on long-term annealing, merging of crystalline blocks and lateral crystal growth at the crystallization temperature, for explaining the observed increases of the crystallinity and melting temperature, are suggested. Though there is detected a large rigid amorphous fraction in PBS crystallized at high supercooling, vitrification only occurs continuously on cooling, after the isothermal crystallization process.

1. Introduction

Poly (butylene succinate) (PBS) is a thermoplastic polyester which gains increasing industrial and public attention because of its sustainability from the points of view of both production and after-use properties. Specifically, PBS may completely be synthesized based on short-term renewable sources, classifying it then as a biopolymer, and it degrades at environmental conditions. Therefore, PBS is attractive for numerous commodity and engineering uses and finds application as packaging material, for mulch films in agriculture, or as biodegradable implant in human bodies, to name only a few [1–8]. The performance of PBS as a material in such applications crucially depends on the presence of a solid crystalline phase after manufacturing, due to its low glass transition temperature T_g of only about −30 to −40 °C [9–12].

Crystallization of polymers, in general, is a multi-step process, proceeding via crystal nucleation, primary and secondary crystallization. Primary crystallization often denotes relatively fast space-filling spherulitic growth of crystals/lamellae while secondary crystallization refers to slow perfection of existing crystals, including lamellar thickening, or formation of additional small crystals in amorphous regions between crystals grown during primary crystallization, termed insertion crystallization [13,14]. PBS crystallizes moderately fast below the equilibrium melting temperature $T_{m,0}$ of around 130 °C [11,12,15–17], with a minimum half-time of crystallization of about 1–10 s slightly above room temperature [18,19]. Melt-crystallization at low supercooling proceeds by growth of lamellae and formation of spherulites [20–22], with the chains arranging in a monoclinic unit cell [23,24]. The maximum crystal fraction is lower than 50% [16,25], which may be caused by the inability of molecular segments for intra-crystalline chain-sliding diffusion [26]. Lamellae growing at low melt-supercooling are thin, with a thickness well below 10 nm [16,27], and melt within few kelvin above the crystallization temperature [28], if

* Corresponding author.
** Corresponding author.
E-mail addresses: rene.androsch@iw.uni-halle.de (R. Androsch), christoph.schick@uni-rostock.de (C. Schick).

https://doi.org/10.1016/j.polymer.2023.126311
Received 29 July 2023; Received in revised form 29 August 2023; Accepted 1 September 2023
Available online 1 September 2023

crystal reorganization is outpaced by fast heating [29–31]. Otherwise, on slow heating, occurs both lamellar thickening and crystal-melting followed by melt-recrystallization [32].

While crystallization of PBS at low melt-supercooling seems well investigated, information about structure formation at temperatures lower than about 60–80 °C are barely available. This holds for morphological data like the size, habit, and higher-order organization of crystals, their structure, or their capability for reorganization. Such information, however, may be of particular importance for practical reasons since conventional melt-processing of PBS via extrusion, injection molding, or blow-molding typically involves fast cooling and solidification at low temperatures [33–38]. In general, as has been confirmed for many different polymers, crystallization at low temperatures often proceeds by homogeneous crystal nucleation, and therefore semicrystalline morphologies are then qualitatively different compared to morphologies obtained after crystallization at high temperature [39–43], affecting properties [44–47].

Primary crystallization of PBS at low temperature, at around T_g (−35 °C), was analyzed regarding its kinetics using fast scanning chip calorimetry (FSC). The study revealed that glass-crystallization is preceded by enthalpy relaxation —as found for many polymers [48]—, and that crystallization near the glass transition temperature leads to formation of crystals of low stability subjected to distinct reorganization during heating [49]. Our own efforts towards analysis of crystallization of PBS at relatively low temperatures included an investigation of the melting behavior of crystals formed at 40 °C, that is, at a temperature near the temperature of maximum crystallization rate [50], with the purpose to unravel the complicated multiple melting characteristics of PBS [51]. It was shown that melting, similar as on high-temperature crystallization [28], occurs slightly above the crystallization temperature, and that the observed weak endothermic peak in differential-scanning-calorimetry (DSC) heating scans of PBS near the crystallization temperature is not caused by relaxation of a rigid amorphous fraction (RAF) [51]. Note that an RAF often develops in semicrystalline polymers in conjunction with crystals [52,53] and has also been detected in PBS [54–57]. Absence of RAF-enthalpy-recovery peaks in DSC heating scans, in addition, was confirmed within a separate study of the origin of so-called annealing peaks in PBS that first was crystallized at high temperature and subsequently annealed at lower temperature [58]. It is anticipated that during low-temperature annealing, after primary crystallization at high temperature, occurs (secondary) insertion crystallization [59–61], promoted by the rather low crystallinity and absence of thickening of lamellae formed during primary crystallization. In a further work, low-temperature secondary crystallization in the glassy state was proven for PBS crystallized at 90 °C, speculating that it may include a transition of RAF into crystalline structure at the surface of pre-existing crystals [9].

In this study, we present further results about crystallization of PBS at low temperature, attempting to provide information about the semicrystalline morphology after primary crystallization, the mechanism of secondary crystallization at the temperature of primary crystallization, and the perfection of crystals. Specific questions include whether (i) low-temperature crystallization yields non-lamellar crystals due to an increased density of homogeneous nuclei, like in isotactic polypropylene (iPP) [62–64], or polyamides (PA) [65–67], (ii) thin lamellae, growing at low temperature, are subject of thickening, that is, if chain-sliding diffusion depends on the thickness of lamellae, and (iii) PBS forms disorder crystals as many other polymers including poly(lactic acid) [68,69], iPP [70,71], PA [66,72,73], or poly(ε-caprolactone) (PCL) [74]. Due to the rather high cooling rate of at least 70 K/s [49], needed to reach low crystallization temperatures, FSC [75] is used as an advantageous tool for both calorimetric analysis of the stability of crystals and sample preparation for classical methods of structure characterization, in particular microscopy [76–78].

2. Experimental

2.1. Material

A fully bio-sourced extrusion-grade PBS homopolymer from MCPP Germany GmbH was used. The melt-flow rate of this polymer is 5 g/(10 min) (190 °C, 2.16 kg) [79] and its mass-average molar mass is 123 kg/mol [80]. The material was delivered in form of pellets and was either processed to films, or used as-received for FSC sample preparation, as described below.

2.2. Film sample preparation

Selected crystallization routes were performed on film samples, for the sake of confirming results obtained on samples prepared in an FSC. A film-maker tool (Specac Ltd., Orpington, UK) in combination with a heatable hydraulic press (LOT QD, Darmstadt, Germany) served for preparing films with a thickness of 200 μm. PBS pellets were placed between fiberglass coated/reinforced Teflon sheets, melted by heating to 150 °C and then shaped to a film. Then, the PBS-film/Teflon sandwich was either directly transferred from the die of the press into an oven (Memmert GmbH, Büchenbach, Germany), pre-conditioned at 100 °C, or quenched in cold water, to allow high- and low-temperature crystallization, respectively. In both cases, different crystallization times were realized, to evaluate the effect to secondary crystallization on the structure. After crystallization, the film, which was prepared in the oven at 100 °C, was rapidly cooled to room temperature, to hinder continuation of ordering during cooling. The thermal history imposed to the films was checked by inserting a K-type (chromel-alumel) microthermocouple (Omega Engineering GmbH, Deckenpfronn, Germany) into the film, to monitor the temperature-time profile during compression-molding, crystallization and subsequent quenching, using a fast OM-DAQXL-1-EU data logger (Omega Engineering GmbH, Deckenpfronn, Germany).

2.3. Instrumentation

Fast scanning chip calorimetry (FSC). A Flash DSC 1 (Mettler-Toledo, Greifensee, Switzerland) was employed for preparation of PBS samples subjected to well-defined crystallization protocols and for calorimetric analysis of subsequent melting and crystal reorganization. The instrument was coupled to an intracooler TC100 (Peter Huber Kältemaschinenbau SE, Offenburg, Germany), to allow sub-ambient temperature operation and fast cooling. The sample compartment of the FSC was purged with gaseous nitrogen at a flow rate of 35 mL/min. Specimens with a typical mass of the order of magnitude of 150 ng were placed at the center of the used UFS 1 chip sensors, where lateral temperature gradients were proven negligible [81].

Preparation of specimens for FSC measurements included microtoming pellets to obtain sections with a thickness of around 8 μm, using a steel-knife-equipped rotary microtome CUT 5062 (Slee medical GmbH, Nieder-Olm, Germany), and subsequent reduction of their lateral size to 50–100 μm using a scalpel and an SMZ series stereomicroscope (Nikon Europe BV, Amstelveen, The Netherlands). Further, general information about FSC sample preparation and operation is reported elsewhere [82].

Atomic force microscopy (AFM). The crystal morphology of PBS crystallized at different conditions was evaluated using a Dimension FASTSCAN AFM (Bruker, Billerica, MA, USA) applying peak-force tapping mode with a peak-force set point of 20 mV. Silicon nitride SCANASYST-FLUID + sensors (Bruker, Billerica, MA, USA) with a nominal spring constant and tip radius of 0.7 N/m and 2 nm, respectively, were employed. Imaging of FSC samples required destruction of the UFS 1 sensor such to remove the ceramic frame from the Silicon nitride membrane where the sample is located. As such, the sample-loaded UFS 1 sensor was first gently pressed with its backside on double-sided sticky tape placed on a glass coverslip, and then the sensor membrane was cut

using a sharp needle at its boundary to the ceramic frame. Afterwards, the frame was removed and the sample, still on the sensor membrane, remained on the tape, ready for imaging.

Polarized-light optical microscopy (POM). The micrometer-scale superstructure of PBS crystallized in the FSC was monitored with an OPN-184 POM (Kern & Sohn GmbH, Balingen, Germany) operated in reflection mode using polarized light and crossed polarizers, with the samples not detached from the sensor for imaging. A DFK 33UX252 camera served for imaging (The Imaging Source Europe GmbH, Bremen, Germany).

The growth rate of PBS spherulites was analyzed using a DMRX microscope (Leica, Wetzlar, Germany) in transmission mode, using a THMS600 hotstage (Linkam, Tadworth, UK). Sections with a thickness of 10 μm were prepared from the pellets with a CUT 5062 microtome equipped with a tungsten carbide knife, and placed between crossed polarizers for investigation. Images were obtained with a Motic camera (Motic Europe, Barcelona, Spain).

Wide- and small-angle X-ray analysis (WAXS and SAXS). WAXS was employed for gaining information about the perfection of crystals forming at different crystallization temperature and to follow the evolution of the crystallinity during secondary crystallization while SAXS served for obtaining knowledge about crystal thicknesses as a function of both the crystallization temperature and time (during secondary crystallization). Experiments were performed in transmission mode using a Retro-F laboratory setup (SAXSLAB, Copenhagen, Denmark) in conjunction with a microfocus X-ray source (AXO Dresden GmbH, Dresden, Germany) and an ASTIX multilayer X-ray optics (AXO Dresden GmbH) as monochromator. We used CuKα radiation (wavelength 0.154 nm), and the diameter of the nearly circular beam was about 0.5 mm. Different exposure times were used depending on the sample-detector distance and sample type/size, and a 2D PILATUS3 R 300K detector (DECTRIS Ltd., Baden, Switzerland) served for registration of the intensity of scattered X-rays. Silver behenate was employed for calibration of sample-to-detector distances. SAXS data were quantitatively evaluated based on modeling the interface-distribution function [83–85], yielding average thicknesses l_c and l_a of stacked crystal lamellae and interlamellar amorphous regions, respectively.

3. Results and discussion

3.1. Kinetics of non-isothermal and isothermal nucleation and crystallization

In this work, the term low-temperature crystallization is applied for temperatures lower than the temperature of maximum crystallization rate, since then crystallization often involves homogeneous crystal nucleation [43]. Pre-requisite for analysis of low-temperature crystallization of PBS is knowledge about the cooling-rate dependence of crystallization, yielding information about the critical cooling rate above which the temperature range of low-temperature crystallization is reached without prior crystallization during cooling the melt. As such, Fig. 1a (left plot) shows the enthalpy of crystallization of PBS as a function of cooling rate, while Fig. 1b (right plot) shows peak-/half-times of crystallization as a function of the crystallization temperature, with the squares/triangles and circles representing data obtained in this work and in the literature [49], respectively. Data are close to each other, that is, the crystallization kinetics of the industrial PBS homopolymer grade of the present study is similar to that of the lab-made grade [49], which probably is also caused by similar molar masses, as indicated in the legend, affecting in particular the crystal growth rate of polymers [86–88]. As such, the critical cooling rate to suppress crystallization is around 100 K/s, and crystallization is fastest slightly above ambient temperature, with the material then crystallizing within 1–2 s. Worth noting is the rather broad minimum of the crystallization peak-/half-time, indicating the overlap of growth- and nucleation-rate contributions. For many polymers, well-separated maxima of crystal-growth- and homogenous-nucleation-rates yield separated minima in the temperature-dependence of the total crystallization time [43,89], which, obviously, is not true for PBS, similar as in the cases of, for example, PCL [90] or poly (ethylene terephthalate) [91, 92].

To shed further light into the temperature-dependence of the total crystallization rate, rates of lateral crystal growth and of crystal nucleation were measured. Fig. 2 shows linear spherulite growth rates, interpreted as lateral crystal growth rate [93], as a function of temperature. Though data obtained on PBS of different molar mass are available in the literature (see light-gray symbols) [16,94], confirming faster growth for PBS of lower molar mass (see light-gray squares), it was our primary goal to gather data at temperatures as low as possible, to eventually observe the temperature of maximum growth rate. Despite

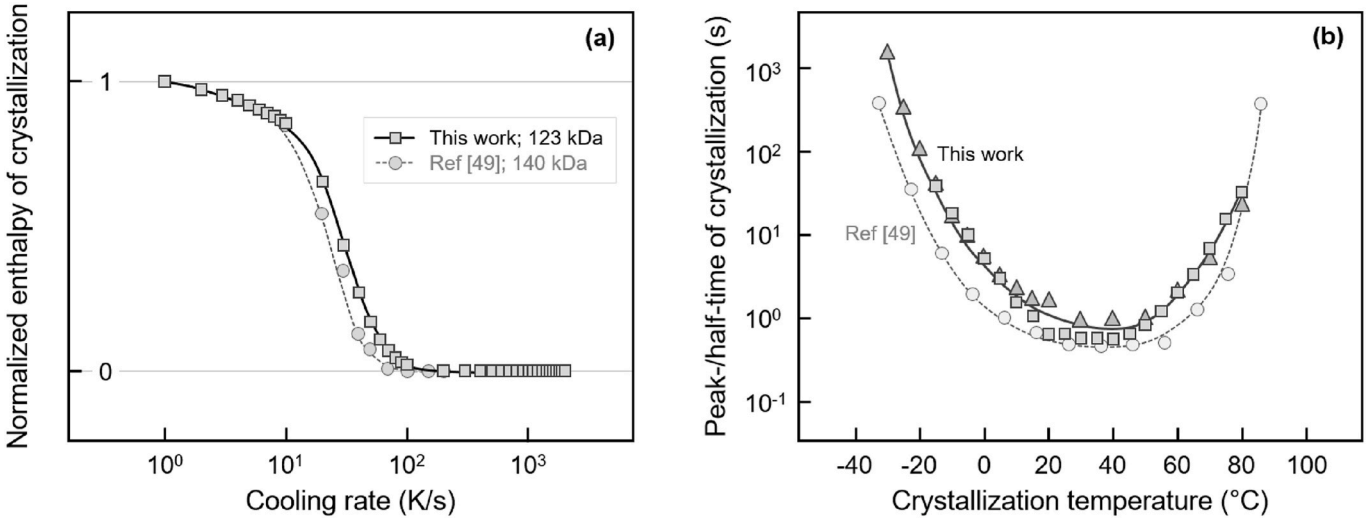

Fig. 1. (a) Normalized enthalpy of crystallization as a function of cooling rate, and (b) peak-/half-time of crystallization as a function of the crystallization temperature of PBS (right). Squares and triangles represent peak- and half-times of crystallization of two independent measurements in this work, respectively, while circles represent data available in the literature [49]. Regarding the latter, y-axis scaling in the left plot is arbitrary since original data were not normalized.

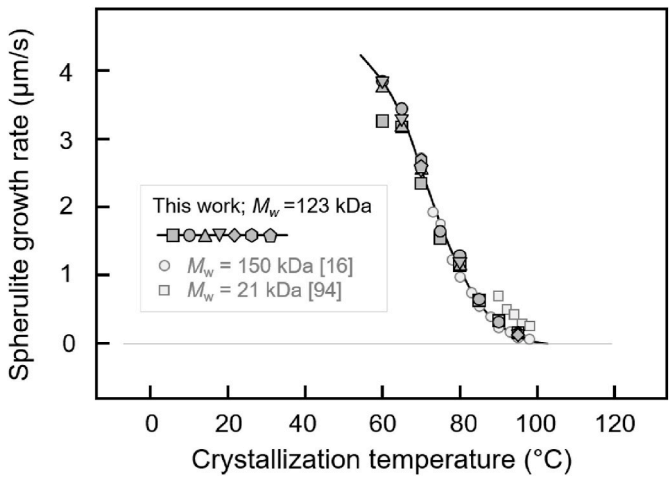

Fig. 2. Spherulite growth rate of PBS as a function of temperature. Dark- and light-gray filling of symbols indicates that data were obtained in this work, or from the literature [16,94], respectively. Regarding the data obtained in this study, different symbols represent different measurements, for demonstrating the reproducibility of data.

being able to widen the temperature-range of existing experiments toward lower temperature, from 70 °C [16] to 60 °C, the temperature of maximum growth rate still was not reached, due to the relatively high number of nuclei and fast filling of space initially not covered by spherulites. However, the data suggest that the temperature of maximum growth rate is well below 60 °C.

Estimation of the kinetics of crystal nucleation included analyses of the effects of cooling rate and of temperature, following Tammann's two-stage crystal nuclei development method [95]. Regarding cooling rate, the data of Fig. 1 provided evidence that cooling the isotropic melt of PBS faster than about 100 K/s suppresses crystal formation. However, even if the melt is cooled faster than 100 K/s, then homogeneous crystal nuclei may form with their number depending on the cooling rate. In analogy to experiments performed on PA 11 [96] and PCL [97,98], PBS was subjected to a wide range of cooling and heating rates in the FSC, to analyze non-isothermal cold-crystallization as a measure of the nuclei number formed in the preceding cooling step. Fig. 3a shows the total enthalpy-change (top sets of data) and the enthalpy of cold-crystallization (bottom sets of data) of PBS during heating at different rates (see legend) as a function of the rate of prior cooling, and Fig. 3b shows the enthalpy of cold-crystallization at an enlarged scale. The total-enthalpy change during heating PBS cooled at different rate (left plot, top part) is equivalent to the data of Fig. 1a, revealing that cooling faster than 100 K/s suppresses crystallization, and that primary and secondary crystallization occur on cooling slower than 100 and 10 K/s, respectively, as concluded from the change of slope of the data sets. Furthermore, the total-enthalpy change is independent of the applied heating rate since this quantity probes the crystallinity before heating.

The bottom part of the left plot as well as the right plot in Fig. 3 show the enthalpy of cold-crystallization during heating at different rates as a function of the prior cooling rate. The observed cooling-rate dependence of the cold-crystallization enthalpy reveals four ranges (I–IV, see right plot), which in the following are explained on the example of the data measured on heating at a rate of 150 K/s. In the cooling-rate range, which allows completion of primary crystallization, that is, after cooling at rates lower than about 10 K/s, distinct cold-crystallization on heating is absent (range I). If primary crystallization during cooling is incomplete, as evident for the cooling-rate range from 10 to 100 K/s (range II), then subsequent heating allows continuation of primary crystallization process by cold-crystallization, enhancing with cooling rate up to 100 K/s due to the increasing amorphous fraction and a sufficient number of nuclei available for crystallization. If the cooling rate is increased further, then, however, decreases the cold-crystallization enthalpy (range III, see arrow) being caused by a lowering of the number of homogeneous crystal nuclei forming during the cooling step. Finally, cooling at rates in range IV has no effect on the cold-crystallization enthalpy on heating, pointing to crystallization initiated by permanently present, heterogeneous crystal nuclei [96–98]. Inspection of the heating-rate dependence of the cold-crystallization process reveals that cold-crystallization is completely suppressed on heating faster than about 500 K/s, enhances on lowering the heating rate from about 500 to 100 K/s, and is then again independent on the heating rate if being lower than 100 K/s. This behavior reflects the kinetics of crystal growth, as, regardless of the number of nuclei, fast heating inhibits their growth and slow heating even allows completion of crystallization without the need of prior formation of homogenous nuclei during cooling. Main result of the experiment described with Fig. 3 is the observation of a critical cooling rate of about 2000 K/s, needed to suppress formation of homogenous crystal nuclei.

The above-described experiments provided information about the

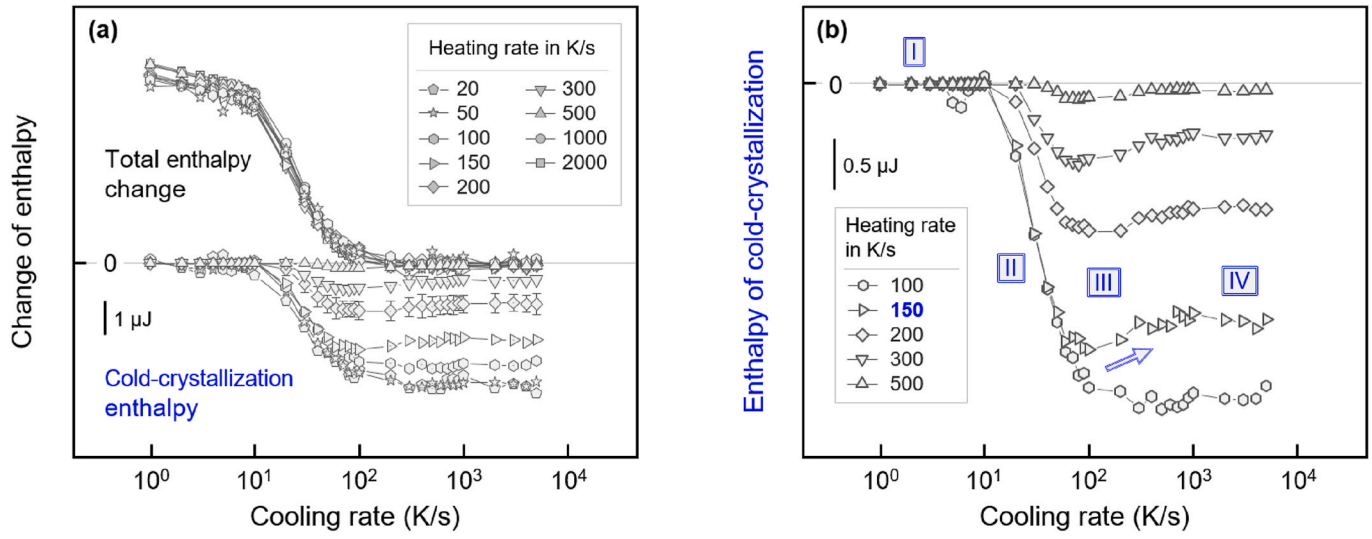

Fig. 3. (a) Total-enthalpy change (left plot, top sets of data) and enthalpy of cold-crystallization (left plot, bottom sets of data) of PBS during heating at different rates (see legend) as a function of the rate of prior cooling. Note that cold-crystallization on heating at 1000 K/s, or faster, is not observed, with the corresponding data (zero cold-crystallization enthalpy) not shown in the lower panel. (b) Enthalpy of cold-crystallization as a function of cooling rate at an enlarged scale.

critical rates of cooling below which crystallization and crystal nucleation occur. However, the applied experimental protocols do not yield information about the temperature range of crystal-nuclei formation if the melt is cooled at rates which allow nucleation but suppress crystallization; note that the temperature-range of crystallization typically is determined by direct analysis of exothermic crystallization peaks in the cooling scans, while nuclei formation does not cause measurable heat flow during cooling. To obtain knowledge about the temperature range of crystal-nuclei formation during cooling, a rather unconventional thermal analysis protocol is applied, shown in Fig. 4a. As such, the melt was cooled at rates of 500 and 1000 K/s —allowing crystal nucleation but suppressing crystal growth— to different minimum temperatures of the cooling step (see blue segment), serving as parameter of the experiment. The number of nuclei forming during cooling is then analyzed as a function of the minimum temperature, by as-fast-as-possible transfer to the growth stage of 70 °C to avoid further structural changes during heating [99–102], and measurement of the enthalpy of cold-crystallization for pre-defined times of 0.5 and 1 s. A similar strategy of analyzing the temperature-range of non-isothermal crystal nucleation has been reported for slowly crystallizing PLLA, using conventional DSC [103], however, is applied here for PBS, using FSC.

Fig. 4b shows in the top part enthalpies of crystallization at 70 °C for 0.5 and 1 s as a function of the minimum temperature, with samples cooled either at 500 or 1000 K/s. The data reveal a major increase of the crystallization enthalpy, that is, of the nuclei number during prior cooling, on decreasing the minimum temperature of the cooling segment to below about 50 °C. The increase turns into a plateau and at minimum temperatures lower than about −20 °C, the nuclei number remains constant. In other words, at temperatures lower than −20 °C, crystal nuclei do not form anymore when PBS was subjected to cooling at 500 or 1000 K/s. Data are further quantified by fitting them with sigmoidal functions (see lines) and calculation of their first derivatives, shown in the bottom part of Fig. 4b. The observed maxima, all located between about 5 and 20 °C, are interpreted as temperatures of maximum nucleation rate. As expected, the plateau-crystallization enthalpy is larger in case of the longer growth stage (see top data), however, with the reason for the slight shift of the upturn of the enthalpy of crystallization (including the maxima in the first-derivative curves) by about 10–15 K to lower minimum temperatures in case of the shorter growth stage not clear yet. In addition, using a lower cooling rate causes an increase of the plateau-enthalpy of crystallization, and also a minor shift of the obtained data sets to lower minimum temperatures, both due to the time- and therefore cooling-rate-dependence of the nucleation process. In summary, the experiment of Fig. 4 provides information that homogeneous crystal nucleation seems fastest between about 5 and 20 °C, about 40–50 K higher than T_g.

Finally, regarding analysis of the kinetics of nucleation, characteristic nucleation times were estimated for temperatures between −50 and 0 °C, with the experimental protocol shown in Fig. 5a. The melt was cooled at 5000 K/s to the nucleation temperature, annealed for different times, and then transferred to the growth temperature of 70 °C to allow crystallization for a pre-defined time of 0.5 s. The effect of the nucleation time on the crystallinity, in units of a change of the enthalpy, shows Fig. 5b. The data reveal begin of nucleation at −50 °C after about 50 s and a decrease of the nucleation onset time with temperature. At 0 °C, nucleation begins already within 0.01 s. It is worth noting that at all analyzed temperatures, short after beginning of nucleation, crystallization/growth occurred, limiting the time-range of analysis of the nucleation kinetics and observation of half-times. For example, at 0 °C, the crystallization half-time is around 1 s (see Fig. 1b), and therefore Fig. 5b only contains data of samples annealed for shorter time up to 0.5 s. Furthermore, it is emphasized that the experiment of Fig. 5 only probed formation of nuclei with a size allowing for growth at 70 °C, while smaller nuclei may have been destroyed during their fast transfer at 5000 K/s to the growth stage.

The estimation of the temperature-dependence of characteristic nucleation times of PBS with the experiment of Fig. 5 is in agreement with the non-isothermal tests of Fig. 4. Both experiments suggest a maximum nucleation rate at a temperature higher than 0 °C, with nuclei formation beginning within few milliseconds. A similar conclusion of fast homogenous nuclei formation close to ambient temperature was derived in an independent work about crystallization of PBS nanocomposites where heterogeneous nucleation by the nanofillers was outpaced by homogenous nucleation at temperatures lower than 10 °C [49]. Fig. 6 summarizes characteristic times of both nucleation and crystallization of PBS as a function of temperature, which in addition reveals information that the kinetics of nucleation is not affected by the glass transition. Data observed below and above T_g fit a single

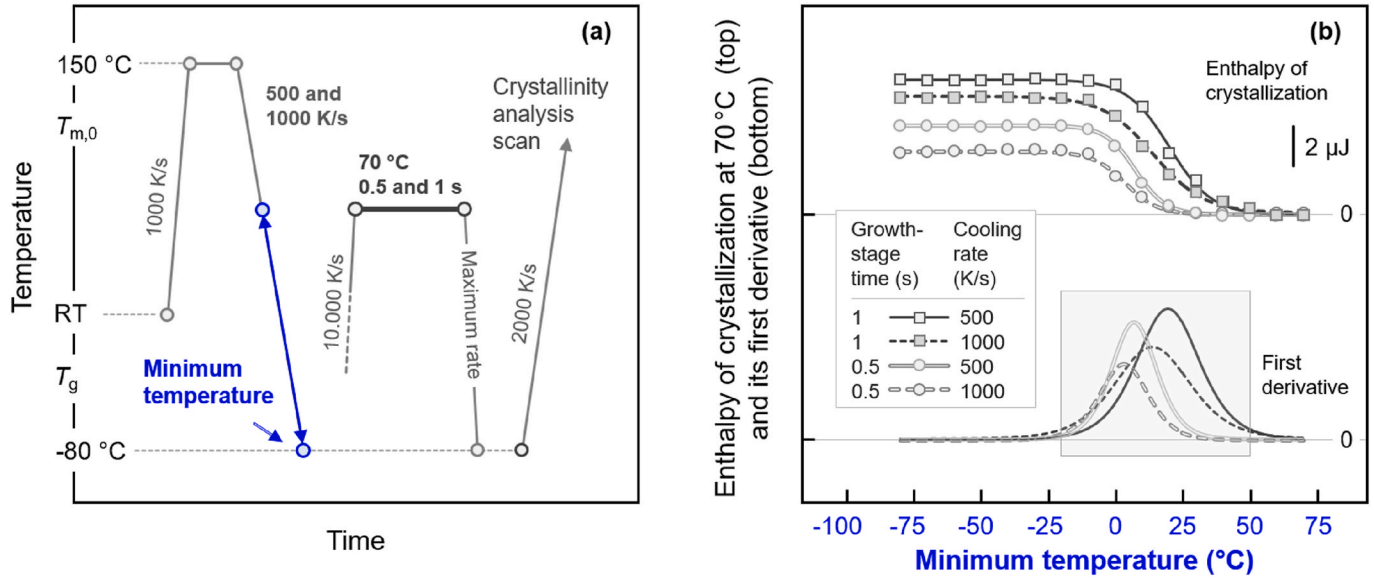

Fig. 4. (a) Temperature-time profile for analysis of non-isothermal nuclei formation in PBS during cooling at 500 and 1000 K/s to a minimum temperature between −80 and 70 °C using an isothermal nuclei-development stage in Tammann's method. (b) Enthalpy of isothermal cold-crystallization at 70 °C for 0.5 s (circles) and 1 s (squares) as a function of the minimum temperature of the nucleation stage, after cooling the melt at 500 and 1000 K/s (top), and first derivatives of their sigmoidal fits (bottom).

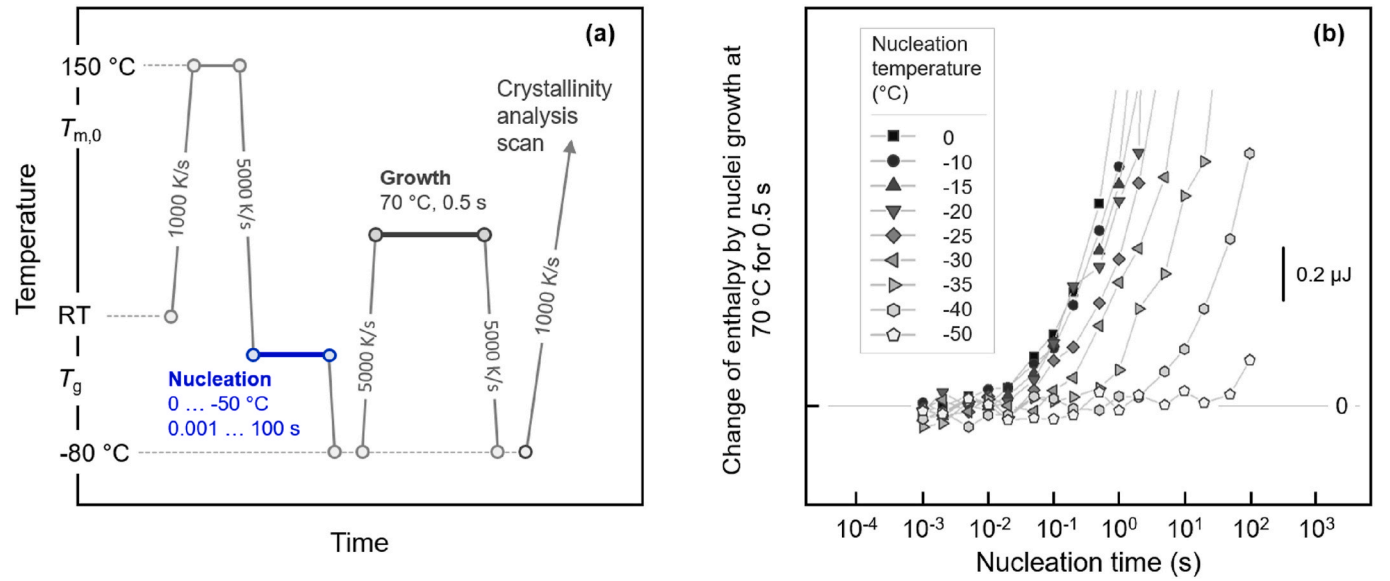

Fig. 5. (a) Temperature-time profile for analysis of isothermal nuclei formation in PBS at temperatures between −50 and 0 °C including isothermal nucleation and growth steps. (b) Change of enthalpy during isothermal cold-crystallization at 70 °C for 0.5 as a function of the time of nucleation at different nucleation temperatures, as indicated in the legend.

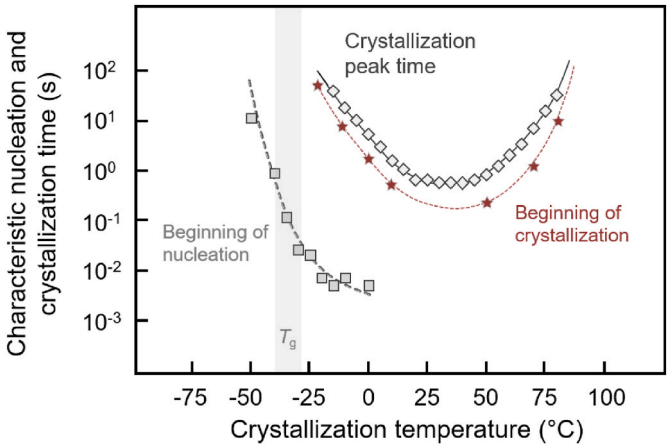

Fig. 6. Characteristic times of nucleation and crystallization of PBS as a function of temperature.

relationship, suggesting that the length scale of molecular mobility required for nuclei formation is shorter than the length scale of the main glass transition, confirming results of an earlier study of nucleation in polyamide 6 [104].

3.2. Crystal morphology and superstructure

To date, information about the crystal morphology and superstructure of PBS are only available for samples crystallized well above ambient temperature, revealing formation of lamellae [21,22,105], and of spherulites [18,20,22,49,105–108]; only in a single study spherulitic growth at 25 °C was detected [109]. For this reason, in the present work, PBS was subjected to low-temperature crystallization in an FSC, with this instrumentation needed to bypass any high-temperature nucleation/crystallization on cooling the melt to the temperature of interest. Fig. 7 shows in the left part the temperature-time profile for crystallization of PBS at 40 °C (red segment) and −30 °C (blue segment). In both cases, crystallization was performed for 5000 s, assuring completion of the primary crystallization process (see also Fig. 1b). After the crystallization step, samples were either cooled from 40 °C at 2000 K/s or

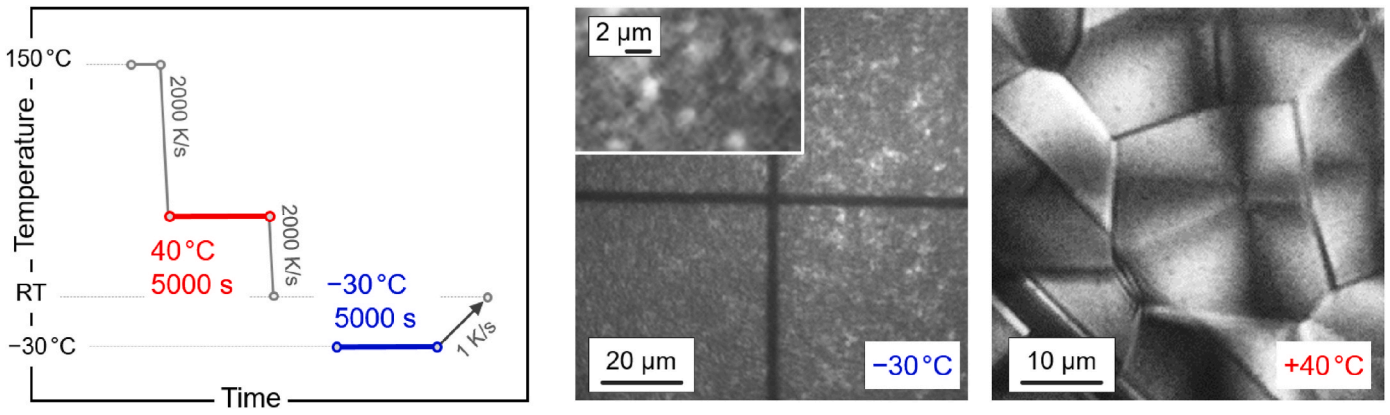

Fig. 7. FSC temperature-time profiles for preparation of PBS samples for microscopic observation of their micrometer-scale morphology after crystallization for 5000 s at 40 °C (red segment) and −30 °C (blue segment) (left). The left and right images show the POM structure of FSC samples of PBS crystallized at −30 and 40 °C, respectively, with the inset in the left image serving to illustrate the small size of birefringent objects. The polarizer directions are parallel to the image borders. (For interpretation of the references to color in this figure legend, the reader is referred to the Web version of this article.)

heated from −30 °C at 1 K/s to room temperature, for microscopic observation. It is not expected that the sample which was crystallized at 40 °C changes its micrometer-scale morphology during cooling, as melting and melt-recrystallization will only occur on heating; at best, insertion crystallization may occur [59–61]. For PBS crystallized at −30 °C, similarly, only local-scale reorganization during slow heating may occur. Therefore, to avoid global melting and melt-recrystallization, a rather low heating rate of only 1 K/s is selected, not affecting the structure at the micrometer length scale. The left and right images of Fig. 7 show the POM microstructure of PBS crystallized at −30 and 40 °C, respectively, revealing qualitatively different morphologies. Crystallization at 40 °C started from few nuclei, which are few ten μm distant from each other, leading to the expected spherulitic morphology. Crystallization at −30 °C, followed by slow heating to room temperature, in contrast, yields a non-spherulitic though not featureless structure in the POM analysis. There are detected numerous birefringent objects/heterogeneities, which presumably are clusters of parallel oriented crystals, with the cluster size being of the order of magnitude of 1 μm or less. Such structure after crystallization near T_g is different from the featureless POM images, observed, for example, for iPP, PA, PCL, or poly (butylene terephthalate) (PBT) [40,74,110,111], and points to either a lower density of homogenous nuclei in PBS, or a high tendency of aggregation/merging of initially smaller domains, as suggested for poly (L-lactic acid) [100].

Information about the crystal morphology of PBS crystallized at different temperatures is provided with the AFM images of Fig. 8, showing the structure after crystallization at −30, 0, 40, and 60 °C (from left to right) at different length scales. As in case of the POM analyses, samples were prepared in an FSC, and red and blue coloring of the crystallization-temperature label indicates that crystallization is assumed being initiated by homogenous and heterogeneous nuclei, respectively, similar as in Fig. 7. Crystallization at 40 and 60 °C led to growth of large spherulites, which advantageously are seen with the two top-row images, showing spherulite boundaries, while at the nanometer length-scale long lamellae are detected. In contrast, crystallization at 0 and −30 °C does not allow formation of large spherulites rather than formation of domains with a size less than a micrometer, decreasing in size and distance between neighbored entities with decreasing crystallization temperature. This observation is in agreement with the left POM image of Fig. 7, which also suggested presence of domains with a similar size. In addition, the two left lower-row images in Fig. 8 provide important information that also low-temperature crystallization via homogenous nucleation ultimately (after heating to room temperature and long-term annealing) yields laterally extended objects, either grown directly or formed by aggregation of initially smaller domains.

3.3. Secondary crystallization of low-temperature crystallized PBS

The relatively fast initial growth of polymer crystals in an isotropic melt and the formation of a space-filled superstructure, often denoted as primary crystallization, may be followed by slower secondary crystallization, involving, for example, isothermal thickening of lamellae or formation of smaller crystals in amorphous structures not occupied by the initially grown primary lamellae on cooling [112–120]. Secondary crystallization in PBS has been suggested valid by analysis of the crystallization kinetics [121] or of the complex melting behavior [17]. Specifically, it has been found that secondary crystallization in PBS proceeds by insertion crystallization —at least during cooling— but not by distinct lamellar thickening [26,58], at least for systems containing crystals formed during primary crystallization at high temperature of 100 °C. In addition, it is worth noting that isothermal crystallization of PBS only produces crystals with a single melting temperature [28,50], that is, crystals of identical stability/size, suggesting absence of insertion crystallization at the temperature of primary crystal growth. In the present study, the initial works reported above are expanded towards analysis of secondary crystallization of PBS after low-temperature primary crystallization.

For illustration of calorimetric detection of secondary crystallization in PBS, Fig. 9a shows FSC heating scans of PBS isothermally crystallized at 20 °C (top set of curves, gray/blue) and 100 °C (bottom set of curves, gray/red), for different time, covering both primary crystallization (gray curves) and secondary crystallization (blue/red curves). Note that in case of crystallization at 20 °C, samples were cooled to −80 °C before heating, while in case of crystallization at 100 °C, samples were heated

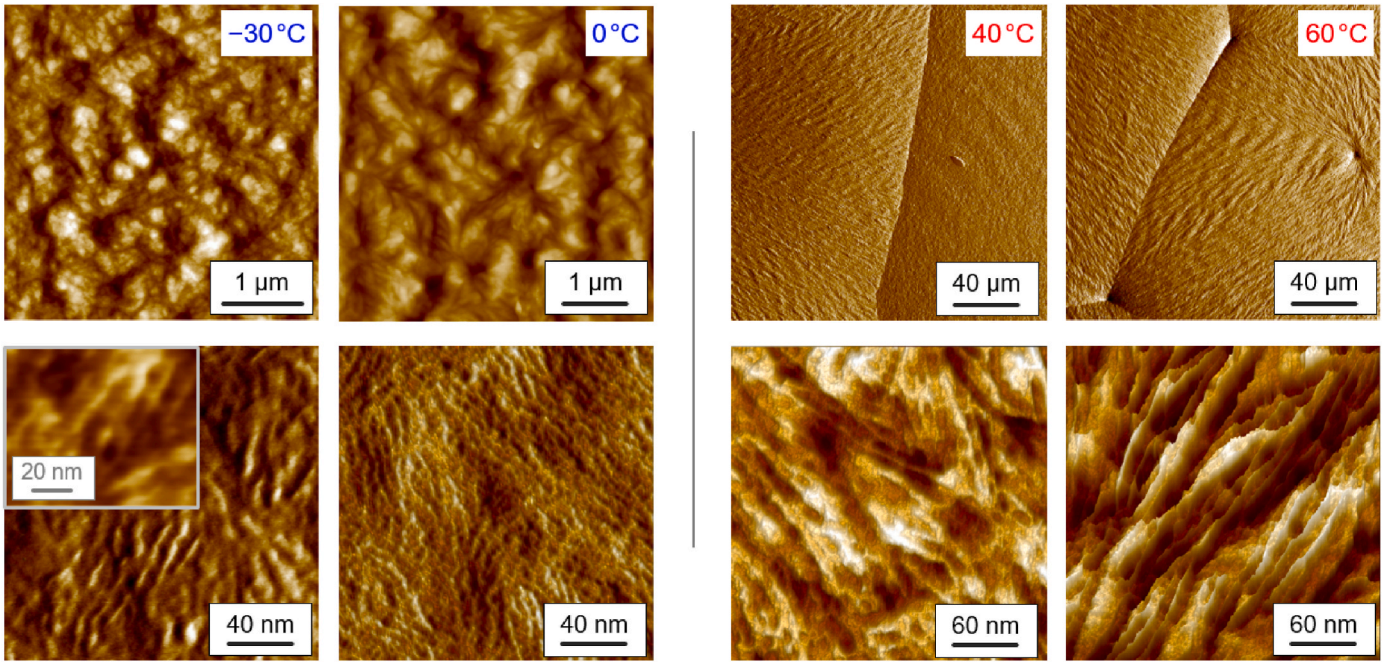

Fig. 8. AFM images of PBS crystallized at −30, 0, 40, and 60 °C (from left to right), prepared by FSC. The upper and lower row images show the structure at the micrometer and nanometer length scales, respectively. Since quantification of the dimensions of structural features (for example the lamellar thickness) is not attempted, both height and error images are employed for qualitative evaluation of morphologies.

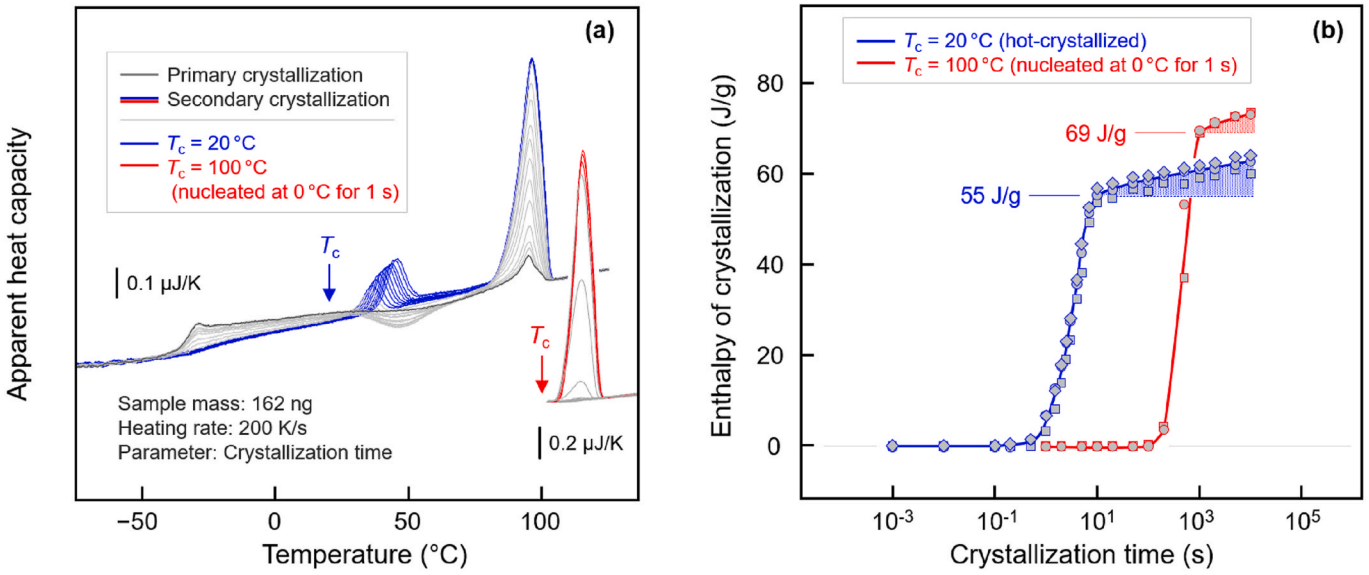

Fig. 9. (a) FSC heating scans of PBS, isothermally crystallized at crystallization temperatures (T_c) of 20 and 100 °C for different time. (b) Enthalpy of crystallization as a function of the crystallization time, obtained by analysis of the change of enthalpy during heating.

immediately after the crystallization step. Furthermore, crystallization at 20 °C started from a melt initially not containing homogenous nuclei, achieved by fast cooling the system from 150 to 20 °C. In contrast, in case of crystallization at 100 °C, an additional nucleation step at 0 °C, lasting 1 s (see also Fig. 6), was included to speed up the crystallization process at 100 °C and to assure reproducibility of the crystallization kinetics. This way, stochastic and non-reproducible high-temperature crystallization in the small FSC sample, related to the low nuclei number when low-temperature nucleation is omitted, can be overcome.

Inspection of the heating curve of PBS annealed at 20 °C for 0.001 s (dark gray curve), being fully amorphous, reveals the glass transition at −30 to −35 °C, which is followed on further heating by a shallow cold-crystallization event —due to the low heating rate of 200 K/s— and a small melting peak. With increasing annealing/crystallization time, first, both the cold-crystallization- and melting-peaks increase in area due to additional formation of nuclei at 20 °C, though crystals are not forming at this temperature yet. Crystal formation at 20 °C is only detected after about 1–2 s, by the decrease of the heat-capacity step at T_g and the evolution of an endothermic (melting) peak slightly above the crystallization temperature T_c. In the early stage of crystallization, up to about 3 s, this peak is difficult to detect, caused by immediate exothermic melt-recrystallization leading to crystals of higher melting temperature. Superposition of melting and melt-recrystallization in FSC heating curves has been illustrated in the literature (Fig. 9 in Ref. [122]), with these two events resolvable by heating faster than a critical rate to suppress recrystallization, in case of PBS at least 20,000 K/s [50]. As will be discussed below, during secondary crystallization (blue curves) the low-temperature melting peak increases in position and area with the time of crystallization, while the high-temperature melting peak is unaffected. Heating of PBS crystallized at 100 °C, without intermediate cooling, and therefore avoiding similar nucleation-related exo- and endothermic events at lower temperature, reveals a single melting peak, scaling in area with crystallization time. Further details about melting and reorganization of PBS crystals formed at 100 °C, not relevant here, are reported elsewhere [28,32].

By analysis of the change of enthalpy during heating of samples crystallized for different time, enthalpies of crystallization are obtained which then are plotted as a function of the crystallization time in Fig. 9b. The data reveal for both crystallization temperatures at first a fast increase of the crystallinity and then a slower process, indicative of primary and secondary crystallization, respectively, with the secondary-crystallization contribution to the overall crystallization enthalpy indicated by shading. Estimation of the sample mass by comparing the measured, absolute value of the heat-capacity increment at T_g on heating fully amorphous PBS (see dark gray curve in the top curve set of Fig. 9a) with the mass-normalized expected value of 0.51 J/(g K) [58,123] yields crystallization enthalpies of 55 and 69 J/g after completion of primary crystallization at 20 and 100 °C, respectively. These values allow an estimation of the crystallinity at the end of the primary-crystallization step by normalizing them with the bulk enthalpy of melting of 200 J/g [12], yielding about 28 and 35% for crystallization at 20 and 100 °C, respectively. Whether the obtained difference of enthalpy-based crystallinities is caused by different crystal fractions or by different degree of order —implying different bulk enthalpy of melting— is unknown.

A further example of FSC analysis of secondary crystallization of PBS is provided with the heating scans of Fig. 10, focusing on the shift of the melting temperature of (non-reorganized) crystals formed at 0 °C (Fig. 10a, left column) and 60 °C (Fig. 10b, right column) with crystallization time. The top, center, and bottom plots show the melting peaks at different temperature resolution, and, in analogy to Fig. 9, gray and blue/red coloring of curves indicates again crystallization-time ranges of primary and secondary crystallization, respectively. In both cases, crystallization at 0 and 60 °C, double melting due to crystal reorganization during heating at 1000 K/s is detected, however, with the low-temperature melting peak —associated to melting of non-reorganized crystals— showing a distinct dependence of the melting temperature on the crystallization time. This observation is in contrast to the high-temperature peak, which stays constant in temperature since the structure of reorganized crystals is only controlled by the heating rate. Closer inspection of the onset of melting of non-reorganized crystals (see center and bottom panels) reveals that the melting temperature only increases during secondary but not primary crystallization (see gray curves, for which the left flank remains unchanged in position). The increase of the melting temperature during secondary crystallization, however, appears depending on the crystallization temperature, which, in the examples of Fig. 10, is indicated for similar annealing times with the gray bar in the bottom plot. As such, for PBS crystallized at 0 and 60 °C, the extrapolated onset of melting of non-reorganized crystals, as illustrated with the tangent construction and arrows in the bottoms plots, shifts within, roughly, two decades (10^1–10^3 s) of crystallization time by around 7 and 5 K, respectively, suggesting a larger increase for

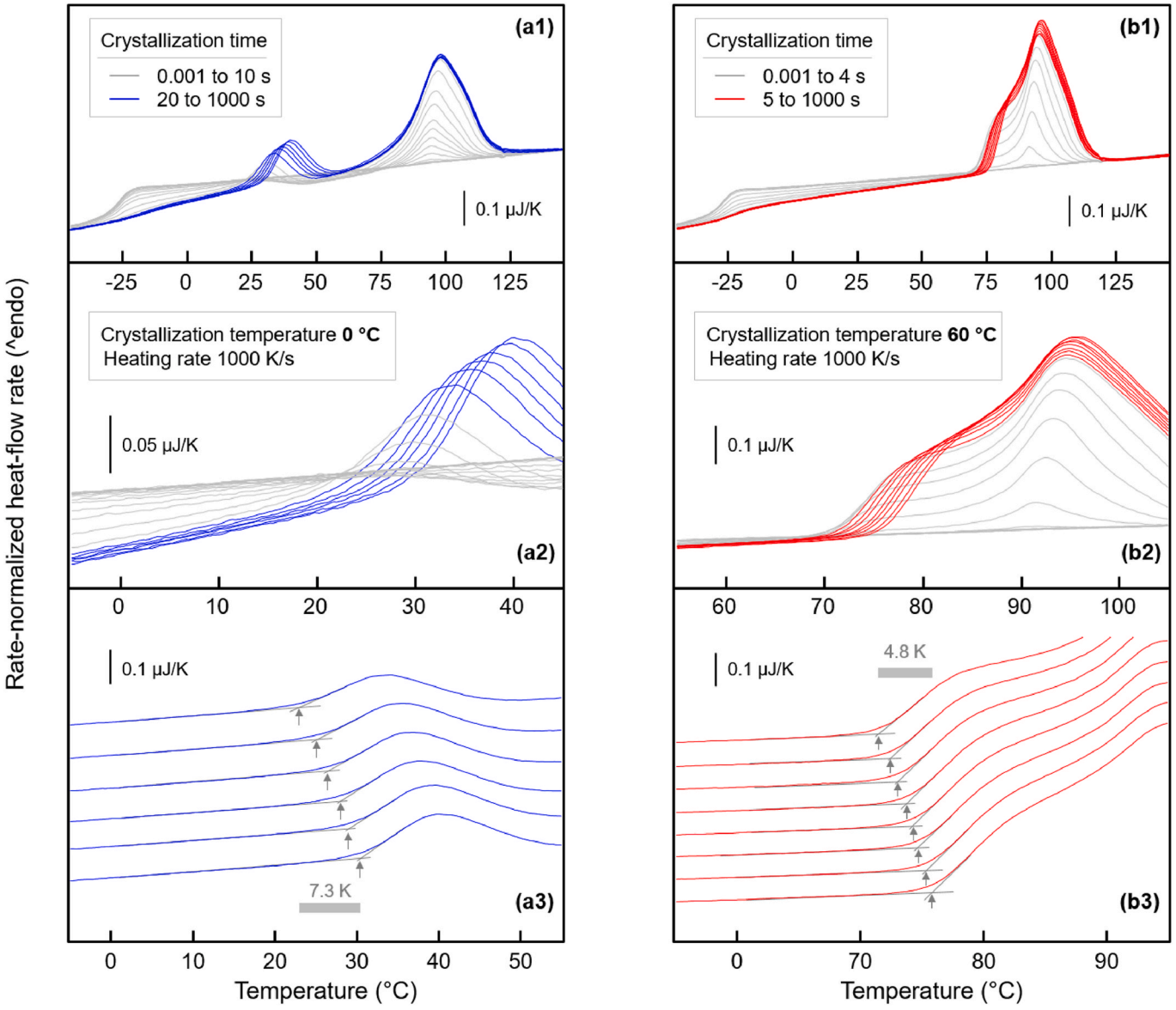

Fig. 10. FSC heating scans of PBS, isothermally crystallized at 0 °C (a1–a3) (left column) and 60 °C (b1–b3) (right column) for different time up to 1000 s. Gray and blue/red coloring indicate time ranges of primary and secondary crystallization, respectively. From top to bottom, the plots show heating scans in different temperature ranges, or stacked, for improved illustration of the estimation of extrapolated onset temperatures of melting, respectively. (For interpretation of the references to color in this figure legend, the reader is referred to the Web version of this article.)

low-temperature crystallized PBS. Important to note, secondary crystallization at the temperature of primary crystallization does not produce a second crystal population of different size/stability and therefore different melting temperature, confirming that the melting-temperature increase is related to a change of the structure formed during primary crystallization.

The experiments of Figs. 9 and 10 represent examples only, with similar data collected in a wide crystallization-temperature range between −20 and 95 °C. Extrapolated onset temperatures of melting of PBS are then plotted as a function of crystallization time within the time-range of secondary crystallization, exemplarily shown with Fig. 11a. The observed increase of the melting temperature (T_m) seems linear with the logarithm of the crystallization time, with such time law often applied to describe the kinetics of secondary crystallization [60, 124–127], though also alternative relations are reported [128]. Note that a detailed analysis of the functional relationship between T_m and crystallization time is beyond the scope of this study, which is also related to the limited time range available for monitoring of annealing effects in the FSC (up to 10,000 s in the present work).

Though difficult to recognize by naked-eye inspection, the increase of T_m with the time of secondary crystallization is larger on crystallization at lower temperature, which is illustrated with the gray lines in the lower part of the Figure, comparing the increases/slopes at −10 and 80 °C. Quantitative information about the increase of the onset melting temperature per decade crystallization time during secondary crystallization as a function of the crystallization temperature is provided with Fig. 11b, with the different symbols representing data obtained from FSC heating curves recorded using rates between 20 and 1000 K/s, as indicated in the legend. The reason behind using different heating rates for measurement of melting temperatures is the attempt to exclude errors by different superheating behaviors of crystals formed at different temperatures, caused by possible changes of the melting kinetics [129–132]. Instrumental-thermal-lag errors, in contrast, are negligible due to the low heating rates used and the rather low mass of samples [133–135].

The data of Fig. 11b suggest a decrease of the increase of the melting temperature per unit of time of secondary crystallization with increasing

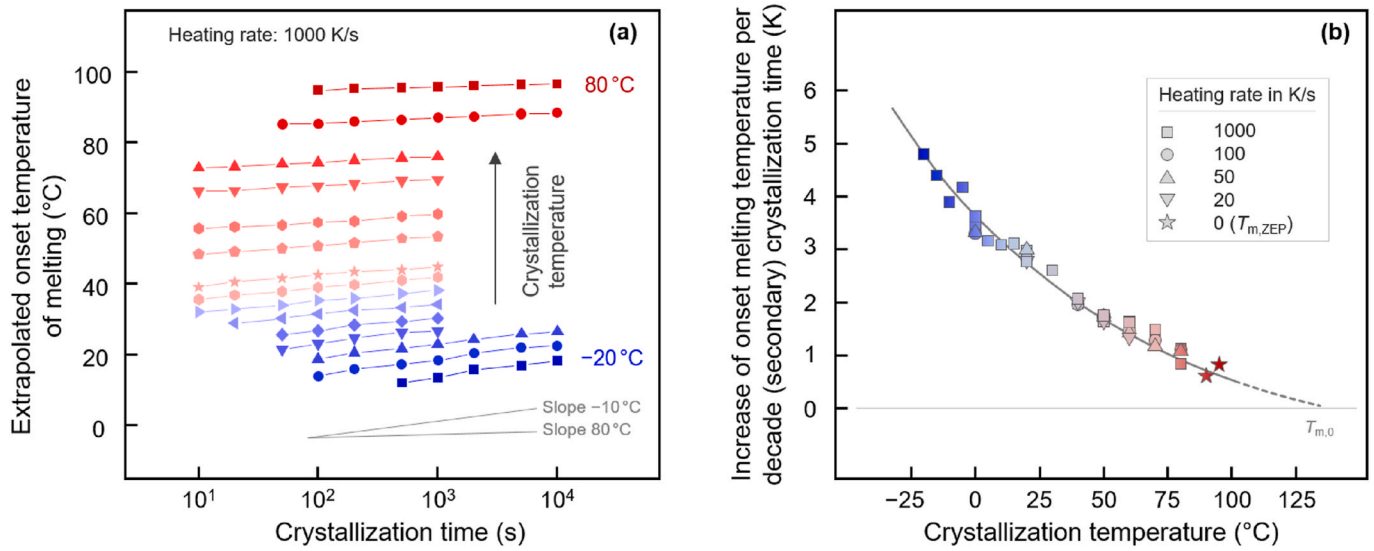

Fig. 11. (a) Extrapolated onset temperature of melting of PBS crystallized at temperatures between −20 and 80 °C as a function of crystallization time, covering the time-range of secondary crystallization. From bottom to top, the different data sets were obtained after crystallization at −20, −15, −10, −5, 0, 5, 10, 15, 20, 30, 40, 50, 60, 70, and 80 °C. (b) Increase of the change of the onset melting temperature per decade crystallization time during secondary crystallization as a function of the crystallization temperature. Data were obtained from FSC heating curves as exemplarily shown in Fig. 10, recorded using different rates, as indicated in the legend. Zero-heating-rate melting temperatures (star symbols) were obtained by extrapolation of sets of melting temperatures measured at different rates, yielding zero-entropy melting temperatures $T_{m,ZEP}$. The line is drawn as a guide for the eye only and is not based on a fit or model.

crystallization temperature. For low crystallization temperatures, slightly above the glass transition, the melting temperature increases by more than 3 K/decade crystallization time, while it approaches a value well below 1 K/decade crystallization time at temperatures higher than 90 °C. Qualitatively, it appears that rather large crystals formed at higher temperature are less prone for secondary crystallization than small crystals formed at lower temperature, with the assumed size-dependence of crystals on the crystallization temperature based on the Hoffman-Lauritzen theory of crystallization [93,136]. Confirming this assumption, extrapolation of the observed dependence toward higher crystallization temperature (see dash line) suggests that equilibrium crystals of infinite size, hypothetically forming at $T_{m,0}$ of around 130 °C [11,12,15–17] cannot stabilize further. The data of Fig. 11b also reveal that variation of the heating rate does not affect the estimation of incremental increase of T_m with the time of secondary crystallization. Note that determination of zero-entropy production melting temperatures ($T_{m,ZEP}$) [29,129,137] requires extrapolation of experimentally observed melting temperatures, measured at different rates, toward zero heating rate and was only applied for selected crystallization temperatures (see star symbols), in analogy to earlier studies of $T_{m,ZEP}$ of PBS [28,50].

In general, the increase of the melting temperature of crystals during secondary crystallization relates to changes of their structure (bulk crystal properties) or their morphology (size, habit, surface structure), as may conveniently be discussed with the Gibbs-Thomson equation (Equation (1)) [137–139]:

$$T_m = T_{m,0}\left[1 - \frac{2}{\Delta h_{m,0}}\left(\frac{\sigma_e}{l_c} + \frac{\sigma}{a} + \frac{\sigma}{b}\right)\right] \quad (1)$$

In equation (1), T_m and $T_{m,0}$ are the experimentally observed melting temperature and equilibrium melting temperature, respectively, $\Delta h_{m,0}$ is the bulk enthalpy of melting, l_c, a, and b are the thickness and the lateral dimensions of the lamellar crystal, respectively, and σ_e and σ are their fold-surface- and lateral-surface-free energies, respectively. Changes of the internal (bulk) structure of crystals during secondary crystallization will cause an increase of both $T_{m,0}$ and $\Delta h_{m,0}$, for example, when slowly transforming a disorder polymorph into a defect-free crystal; a prominent example for such scenario is the α′- to α-crystal transformation on long-term annealing of PLLA at elevated temperature [140–144]. For a crystal, which does not change its bulk properties on secondary crystallization, increases of the melting temperature may then be caused by an increase of its volume-to-surface ratio and/or decrease of the surface free energies. Since the lateral dimensions (a, b) of a lamella are much larger than its thickness (l_c), and since the free energy of the fold surface (σ_e) is higher than that of the lateral crystal faces (σ) [145,146], the last two terms in equation (1) often are omitted, and melting-temperature increases are then discussed being related to lamellar thickening only. In the following section, to identify the reason for the observed increase of the melting temperature of low-temperature crystallized PBS during secondary crystallization, the time dependencies of the bulk crystal structure and lamellar thickness are evaluated.

3.4. Crystal structure and absence of lamellar thickening of low-temperature crystallized PBS during secondary crystallization

Fig. 12a shows WAXS patterns, intensity as a function of the scattering angle 2θ, of PBS crystallized for a period of about 24 h at 100 °C (red curve) and 20 °C (blue curve), with the strong peaks of the sample crystallized at 100 °C indexed based on crystal-structure information available in the literature [24]. Assignment of weak peaks to specific (hkl) is difficult and therefore omitted. Comparison of the X-ray patterns of PBS crystallized at 100 and 20 °C reveals for the latter case less and broader peaks, indicating the formation of imperfect and smaller crystals [147]. In addition is detected a shift of the peaks to lower scattering angles, suggesting an increase of the unit-cell dimensions, at least in cross-chain direction. Further, in-depth conclusions such as whether the low-temperature structure is a specific polymorph forming below a critical temperature, as in PLLA [68,69,148], or whether there is a continuous increase of the degree of disorder with decreasing crystallization temperature, as suggested in an earlier work [17], however, cannot be drawn since requiring more dedicated experiments, out of scope here.

Important for discussion of the increase of the melting temperature of low-temperature crystallized PBS during secondary crystallization (see Fig 11), Fig. 12b shows the evolution of WAXS patterns of PBS crystallized at 20 °C during annealing up to 1440 min (24 h). In detail, a

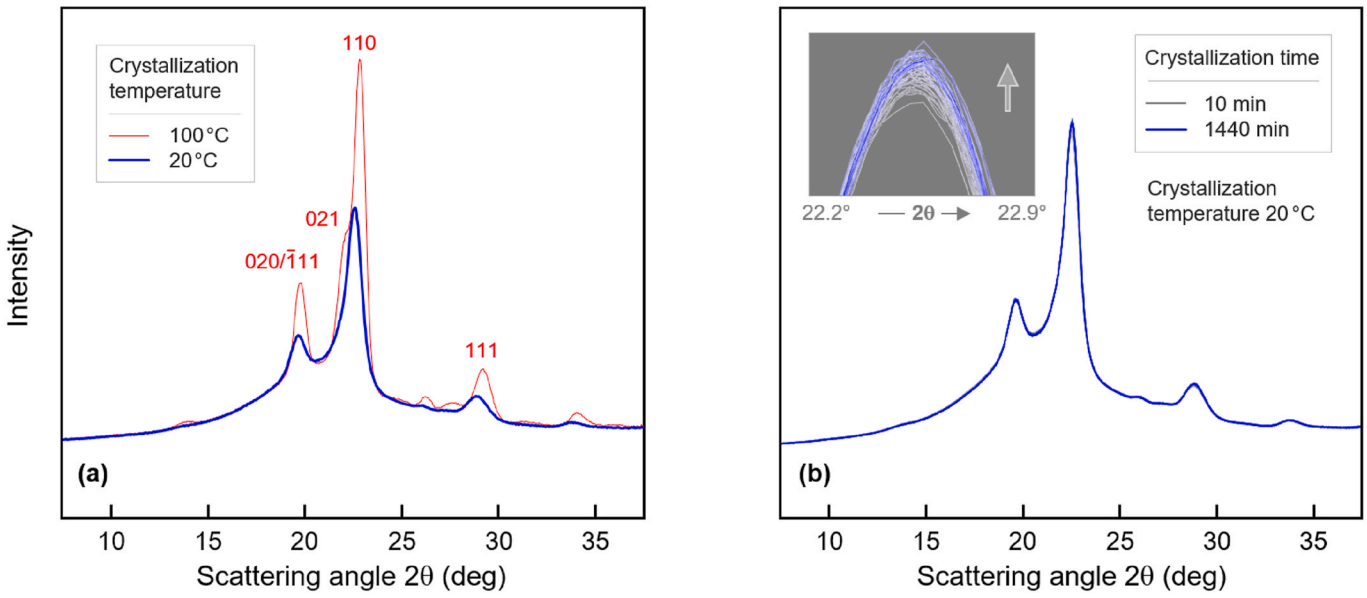

Fig. 12. (a) WAXS patterns, intensity as a function of the scattering angle 2θ, of PBS crystallized at 100 °C (red curve) and 20 °C (blue curve). Indexing is based on crystal-structure information available in the literature [24]. (b) WAXS patterns of PBS crystallized at 20 °C for different periods up to 1440 min (24 h) during secondary crystallization. The inset shows the increase of the maximum intensity of the 110 peak at an enlarged scale during annealing. All measurements were performed on film samples at 20 °C. (For interpretation of the references to color in this figure legend, the reader is referred to the Web version of this article.)

PBS film was quenched to ambient temperature faster than 100 K/s and immediately transferred into the X-ray device. Data collection started after about 300 s, that is, well after completion of primary crystallization (see Figs. 1b and 9b), and the first WAXS pattern was observed after about 600 s. Within 24 h, a total of 45 measurements was performed, with the obtained curves stacked on top of each other. The overview-plot does not reveal qualitative changes of the structure during secondary crystallization, as the number, angular position, and width of the scattering peaks remains unchanged. Close inspection of the evolution of the maximum intensity of the peaks, however, suggests an increase of the crystallinity during secondary crystallization, as is illustrated with the inset in Fig. 12b, showing the increase of the maximum intensity of the 110 peak at an enlarged scale (see vertical arrow). This result is in agreement with the data of Fig. 9b, which proved an increase of the enthalpy-based crystallinity by about 5%, equivalent to an increase of the enthalpy of crystallization from about 55 J/g at the end of primary crystallization to (extrapolated) 65 J/g after 24 h annealing. Regarding the large increase of the melting temperature during secondary crystallization (2–3 K/decade crystallization time), referring to the Gibbs-Thomson equation (Equation (1)), the X-ray data rule out that it is caused by changes of both $T_{m,0}$ and $\Delta h_{m,0}$, as in that case a change of the crystal structure/unit cell would have been expected. In other words, the observed increase of the melting temperature is caused by changes of the size of crystals and/or their surface free energy.

For high-temperature crystallization, lamellar thickening has been excluded as a mechanism of secondary crystallization [26], however, for

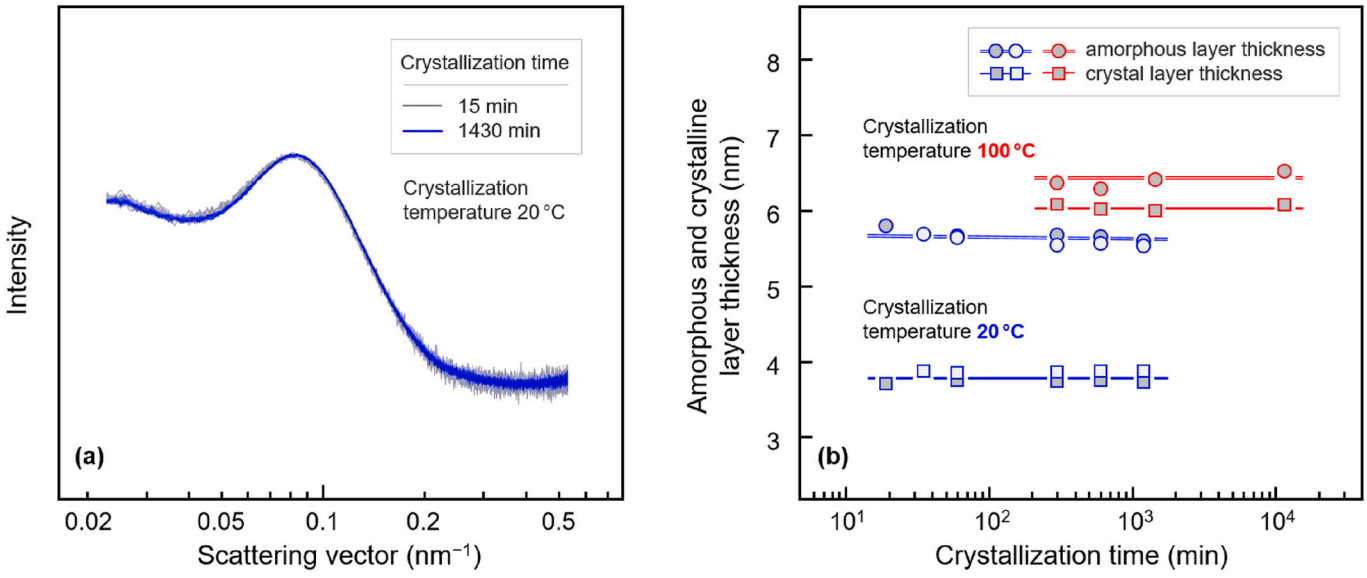

Fig. 13. (a) SAXS patterns, intensity as a function of the scattering vector, of PBS crystallized at 20 °C for different periods up to 1430 min (about 24 h) during secondary crystallization. (b) Amorphous (circles) and crystal (squares) layer thicknesses of PBS crystallized at 20 (blue) and 100 °C (red) for different time during secondary crystallization. The lines are guides to the eye only, and light- and dark-gray-filled blue symbols represent measurements performed on different samples. (For interpretation of the references to color in this figure legend, the reader is referred to the Web version of this article.)

low-temperature crystallized PBS, information about absence of crystal thickening during long-term annealing at the temperature of primary crystallization is not yet available. For this reason, SAXS measurements were performed, using identical samples as employed for WAXS analysis (see Fig. 12). Note that SAXS and WAXS patterns were recorded alternately, with the exposure time reduced for the first 10 (out of the total 45) measurements, to monitor secondary crystallization at shorter time increments in the early stage of secondary crystallization, causing, however, slightly increased noise of raw data. Fig. 13a shows SAXS patterns, intensity as a function of the scattering vector, of PBS crystallized at 20 °C for different periods up to 1430 min (about 24 h) during secondary crystallization, with the curves stacked on top of each other. By visual inspection, it appears that SAXS data are independent of the crystallization time, with the position and intensity of the observed long-period maximum unchanged. Quantitative evaluation of the SAXS curves provides information about the thickness of the amorphous and crystal layers, shown with the blue symbols/lines as a function of the crystallization time during secondary crystallization in Fig. 13b. In addition, for comparison, Fig. 13b also contains data observed on films annealed at 100 °C (red symbols/lines). The thickness l_c of the crystalline lamellae forming at 20 and 100 °C is around 3.8 and close to 6.1 nm, respectively, and does not show, in both cases, an increase during secondary crystallization. Therefore, lamellar thickening is not a valid mechanism of secondary crystallization in PBS crystallized at low temperature, and the increase of the melting temperature during secondary crystallization must be caused by a change of the size of crystals in lateral direction. Furthermore, the experiment of Fig. 13 suggests that intracrystalline chain diffusion, proven absent for lamellae formed at high temperature [26], is not largely affected by the thickness of crystals, at least in the specific case of PBS.

Rough estimation of the linear, volume-based crystallinity [149] yields values of about 40 and 48% for PBS crystallized at 20 and 100 °C, respectively, almost independent of the crystallization time. With the knowledge of the densities of the crystalline and amorphous phases, 1.34 and 1.18 g/cm^3 [12,26], respectively, mass-based crystallinities of about 43 and 52% are observed after crystallization at 20 and 100 °C from the SAXS data, allowing a comparison with enthalpy-based values obtained by calorimetry (see Fig. 9b). For the latter, crystallinities of 28 and 35% were observed after crystallization at 20 and 100 °C for about 24 h, respectively, with these values being distinctly lower than detected by SAXS. The reasons are manifold and briefly discussed as follows, separately for crystallization at 100 and 20 °C.

Regarding crystallization at 100 °C, recently it was found that crystals formed at high temperature may have a lower bulk enthalpy of melting ($\Delta h_{m,0}$) of 183 J/g [26] instead the earlier suggested values of 200 J/g [12], 210 J/g [15], or 213 J/g [150]. Recalculation of the DSC-crystallinity using the lower value of 183 J/g, however, would yield an only slightly higher value of still lower than 40%, thus not providing an explanation of the observed difference between SAXS- and DSC-crystallinities. SAXS data were obtained at ambient temperature, while the DSC-crystallinity holds for the temperature of crystallization of 100 °C. Reversible lamellar thickening [151,152] on cooling PBS after high-temperature crystallization, which would cause an increase of the crystallinity, is excluded since PBS crystals are classified as crystal-fixed [26,153]. However, a major increase of the crystallinity is expected to occur by insertion crystallization on cooling [58], with nuclear magnetic resonance spectroscopy data suggesting an increase of the crystallinity on cooling PBS from 100 to 30 °C by a factor of 1.4 [26]. Such increase of the crystallinity on cooling provides a straightforward explanation of the observed difference between SAXS- and DSC-crystallinities.

Regarding crystallization of PBS at 20 °C, the obtained crystallinity values of 28 and 43% measured by calorimetry and SAXS, respectively, hold both for ambient temperature, that is, the discrepancy cannot be explained by cooling-controlled insertion crystallization. Similar as described above, there exists uncertainty regarding calculation of the enthalpy-based crystallinity since the (unknown) bulk enthalpy of melting of crystals containing defects is expected lower than was used for the calculation (200 J/g). As an analogue, for disorder crystals of PLLA, showing similar absence of selected diffraction peaks, and slight enlargement of the unit cell (see Fig. 12a), compared to the regular crystal structure [69], the bulk enthalpy of melting is about 25% lower [143,154,155]. In addition, a minor error in the calculation of the enthalpy-based crystallinity may be introduced by not considering the temperature-dependence of the bulk enthalpy of melting. Perhaps more important, the rather high SAXS crystallinity may also indicate presence of semicrystalline structure outside lamellar stacks in which the local crystallinity is lower than is probed with the linear stack model.

3.5. Rigid amorphous fraction in low temperature-crystallized PBS

There is an ongoing debate whether so-called annealing peaks in DSC heating scans of semicrystalline polymers, subjected to annealing above T_g, are caused by melting of crystals [58], or by relaxation of a glassy rigid amorphous fraction (RAF) [156–160], with the latter also suggested for PBS [51] and its family member poly (hexamethylene succinate) [161]. Since the FSC heating scans obtained after low-temperature crystallization of PBS show multiple endothermic peaks (see Figs. 9a and 10a), it is attempted ruling out interpretation of the low-temperature event being caused by relaxation of amorphous structure rather than assigning it to melting of originally formed crystals. Fig. 14 shows two FSC scans, recorded on heating PBS melt-crystallized at 20 °C for different time of 0.001 s (gray curve) and 10 s (blue curve), using a rate of 200 K/s. Annealing the supercooled melt at 20 °C for 0.001 s does not allow formation of crystals and the sample remains fully amorphous. The corresponding heating scan, recorded after cooling the sample to −80 °C, then shows the glass transition/devitrification slightly below −30 °C, indicated with the step-like increase of the heat capacity when turning the structure from solid to liquid [162,163]. Isothermal annealing of PBS at 20 °C for 10 s, in contrast, permits completion of primary crystallization (see Figs. 1b and 9b) and, therefore, in the

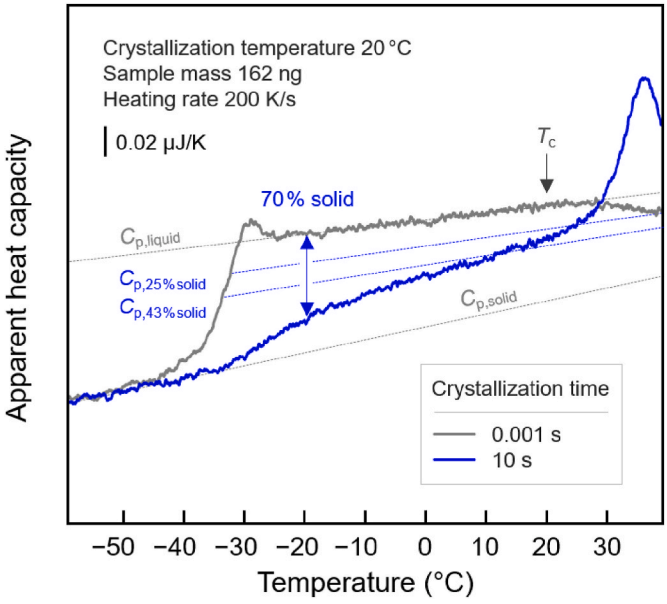

Fig. 14. FSC heating scan of fully amorphous PBS (gray curve) and PBS crystallized at 20 °C for 10 s (blue curve). The dotted gray lines indicate the heat capacity of fully liquid and solid PBS ($C_{p,liquid}$ and $C_{p,solid}$, respectively), linearly extrapolated to temperatures where experimental data are not available. The blue dotted lines, labeled $C_{p,25\%\ solid}$ and $C_{p,43\%\ solid}$, represent the heat capacity above T_g expected for PBS containing 25 and 43% solid fraction. The heating rate was 200 K/s, and the crystallization temperature (T_c) is indicated with the gray vertical arrow. (For interpretation of the references to color in this figure legend, the reader is referred to the Web version of this article.)

subsequently recorded heating scan, the heat-capacity step at T_g is reduced due to the presence of solid crystals. FSC and SAXS analyses (see Figs. 9b and 13b) suggested crystal fractions of 25% (considered as lower limit due to uncertainty regarding the used bulk enthalpy of melting for calculation, and the proven presence of disorder crystals, Fig 12a) and 43% (considered as upper limit if not taking into account semicrystalline structure outside lamellar stacks), respectively. With a remaining amorphous fraction of 57–75%, however, a much larger than observed heat-capacity step is expected at T_g. In fact, the FSC data suggest that only about 30% of the total structure is devitrified at the end of the glass transition, at around −20 °C, and that about 70% remained solid. This mismatch typically is explained by the presence of not-yet-devitrified (rigid) amorphous structure, in the present case, roughly, 30–40% at −20 °C. However, more important in the context of the interpretation of the endothermic peak slightly above the crystallization temperature T_c is the observation of increasing liquid fraction (indicated with increasing difference between the blue curve and gray-dotted line labeled $C_{p,solid}$) with increasing temperature, such that at the crystallization temperature the entire amorphous phase seems de-vitrified/liquid. As such, it appears that any amorphous structure present at the crystallization temperature is in structural equilibrium and that at this temperature relaxation processes are faster than probed by the experiment-time scale. In other words, relaxation of a glassy amorphous phase at T_c is considered disproven, suggesting that the endothermic peak slightly above T_c indeed is caused by melting of crystals. Though not major subject of this study, the FSC heating scan of low-temperature crystallized PBS reveals furthermore that vitrification and devitrification of the RAF is not a discrete event but occurs continuously in a broad temperature range, perhaps indicating a structural gradient between the crystal surface and the bulk amorphous phase. Crystallization during cooling between 20 °C and T_g, and melting during subsequent heating is a further option for explaining the observed FSC curve in this temperature range. However, such increase of the crystallinity from around 30–40% (at T_c) to 70% (at T_g) seems unreasonably high.

4. Conclusions

In this study, melt-crystallization of poly (butylene succinate) (PBS) at high supercooling, that is, at temperatures lower than the maximum crystallization rate, was comprehensively analyzed to yield information about the nucleation and crystallization kinetics, semicrystalline morphologies, and mechanisms about structural changes during long-term annealing/secondary crystallization. Application of Tammann's two-stage crystal nuclei development method in different variations (Figs. 3–5) —(a) non-isothermal nucleation and growth stages, (b) non-isothermal nucleation stage with variation of the minimum temperature followed by an isothermal growth state, and (c) isothermal nucleation and growth stages— suggested that homogeneous crystal nucleation is absent on cooling faster than few 10^3 K/s. Furthermore, it was found that crystal nucleation is fastest near or slightly below ambient temperature, about 40–50 K above T_g. At lower temperatures, the nucleation rate decreases, however, with the glass transition temperature not affecting the observed general temperature-dependence. With earlier similar observations on PCL, PA 6 and poly (butylene isophthalate) [89,90,104,164] it appears therefore settled that cooperative large-scale chain mobility, controlling vitrification and devitrification of amorphous structure on cooling and heating, respectively, does not affect the kinetics of formation of homogenous nuclei.

Crystallization of PBS at low temperature, ultimately, leads to formation of thin lamellae, probably composed of smaller blocks, with a slightly enlarged unit cell compared to crystals grown at high temperature, pointing to presence of conformational crystal defects. The presence of such defects complicates the estimation of the crystallinity by calorimetry when causing a lowering of the bulk enthalpy of melting. Long-term annealing of such defective crystals at the temperature of primary crystallization does not affect their bulk structure (unit cell), implying metastability at the crystallization temperature. This observation is in agreement with absence of lamellar thickening and the proposal that, at least in case of PBS, intracrystalline chain diffusion is independent on the thickness of lamellae.

Isothermal secondary crystallization of PBS at the temperature of primary crystallization does not produce new crystals with a different melting temperature than observed during primary crystallization, however, is connected with a stabilization of existing crystals. The observed distinct increase of the melting temperature is not caused by polymorphic changes and also not by an increase of the lamellar thickness. Applying the exclusion principle and the Gibbs-Thomson equation, crystal stabilization must therefore occur by lateral growth of (initially rather short) lamellae, or merging of crystals at their lateral faces. This statement relies on the reasonable assumption that the specific surface free energies of crystals are not a function of the secondary crystallization time.

CRediT authorship contribution statement

René Androsch: Conceptualization, Investigation, Writing – original draft, preparation, Writing – review & editing. **Katalee Jariyavidyanont:** Investigation, Writing – review & editing. **Andreas Janke:** Investigation, Writing – review & editing. **Christoph Schick:** Conceptualization, Writing – review & editing.

Declaration of competing interest

The authors declare that they have no known competing financial interests or personal relationships that could have appeared to influence the work reported in this paper.

Data availability

Data will be made available on request.

Acknowledgment

KJ and RA acknowledge financial support the by Deutsche Forschungsgemeinschaft (DFG) (Grant Number AN 212/29–1). The authors thank Q. Yu (Martin Luther University Halle-Wittenberg, Institute of Physics) for assistance in SAXS data evaluation.

References

[1] J. Xu, B.H. Guo, Poly (butylene succinate) and its copolymers: research, development and industrialization, Biotechnol. J. 5 (2010) 1149–1163.
[2] O. Platnieks, S. Gaidukovs, V.K. Thakur, A. Barkane, S. Beluns, Bio-based poly (butylene succinate): recent progress, challenges and future opportunities, Eur. Polym. J. 161 (2021), 110855.
[3] S.A. Rafiqah, A. Khalina, A.S. Harmaen, I.A. Tawakkal, K. Zaman, M. Asim, M. N. Nurrazi, C.H. Lee, A review on properties and application of bio-based poly (butylene succinate), Polymers 13 (2021) 1436.
[4] E. Piorkowska, Overview of biobased polymers, Adv. Polym. Sci. 283 (2019) 1–35.
[5] V. Siracusa, N. Lotti, A. Munari, M. Dalla Rosa, Poly (butylene succinate) and poly (butylene succinate-co-adipate) for food packaging applications: gas barrier properties after stressed treatments, Polym. Degrad. Stabil. 119 (2015) 35–1136.
[6] D. Adhikari, M. Mukai, K. Kubota, T. Kai, N. Kaneko, K.S. Araki, M. Kubo, Degradation of bioplastics in soil and their degradation effects on environmental microorganisms, J. Agric. Chem. Environ. 5 (2016) 23–34.
[7] S. Vytejčková, L. Vápenka, J. Hradecký, J. Dobiáš, J. Hajšlová, C. Loriot, L. Vannini, J. Poustka, Testing of polybutylene succinate based films for poultry meat packaging, Polym. Test. 60 (2017) 357–364.
[8] A. Mtibe, S. Muniyasamy, T.C. Mokhena, O.O.V. Ojijo, M. John, Recent insight into the biomedical applications of polybutylene succinate and polybutylene succinate-based materials, Express Polym. Lett. 17 (2023) 2–28.
[9] M.L. Di Lorenzo, R. Androsch, M.C. Righetti, Low-temperature crystallization of poly (butylene succinate), Eur. Polym. J. 94 (2017) 384–394.
[10] F. Signori, M. Pelagaggi, S. Bronco, M.C. Righetti, Amorphous/crystal and polymer/filler interphases in biocomposites from poly (butylene succinate), Thermochim. Acta 543 (2012) 74–81.

[11] J.J. Moura Ramos, H.P. Diogo, Slow relaxations in semicrystalline poly (butylene succinate) below and above T_g, Polym. Eng. Sci. 55 (2015) 1873–1880.
[12] T. Miyata, T. Masuko, Crystallization behaviour of poly (tetramethylene succinate), Polymer 39 (1998) 1399–1404.
[13] G. Strobl, The semicrystalline state, in: The Physics of Polymers: Concepts for Understanding Their Structures and Behavior, 165–222, Springer, Berlin, 2007.
[14] B. Wunderlich, Macromolecular Physics, in: Crystal Nucleation, Growth, Annealing, 2, Academic Press, New York, 1976.
[15] G.Z. Papageorgiou, D. Bikiaris, Crystallization and melting behavior of three biodegradable poly (alkylene succinates). A comparative study, Polymer 46 (2005) 12081–12092.
[16] Z. Gan, H. Abe, H. Kurokawa, Y. Doi, Solid-state microstructures, thermal properties, and crystallization of biodegradable poly (butylene succinate) (PBS) and its copolyesters, Biomacromolecules 2 (2001) 605–613.
[17] E.S. Yoo, S.S. Im, Melting behavior of poly (butylene succinate) during heating scan by DSC, J. Polym. Sci., Polym. Phys. 37 (1999) 1357–1366.
[18] J. Jiang, E. Zhuravlev, W. Hu, C. Schick, D. Zhou, The effect of self-nucleation on isothermal crystallization kinetics of poly (butylene succinate) (PBS) investigated by differential fast scanning calorimetry, Chin. J. Polym. Sci. 35 (2017) 1009–1019.
[19] H.E. Yener, G. Hillrichs, R. Androsch, Phase behavior of solvent-rich compositions of the polymer/drug system poly (butylene succinate) and N, N-diethyl-3-methylbenzamide (DEET), Colloid Polym. Sci. 299 (2021) 873–881.
[20] K.J. Ihn, E.S. Yoo, S.S. Im, Structure and morphology of poly (tetramethylene succinate) crystals, Macromolecules 28 (1995) 2460–2464.
[21] H. Wang, J.M. Schultz, S. Yan, Study of the morphology of poly (butylene succinate)/poly (ethylene oxide) blends using hot-stage atomic force microscopy, Polymer 48 (2007) 3530–3539.
[22] H. Wang, Z. Gan, J.M. Schultz, S. Yan, A morphological study of poly (butylene succinate)/poly (butylene adipate) blends with different blend ratios and crystallization processes, Polymer 49 (2008) 2342–2363.
[23] Y. Ichikawa, J. Suzuki, J. Washiyama, Y. Moteki, K. Noguchi, K. Okuyama, Strain-induced crystal modification in poly (tetramethylene succinate), Polymer 35 (1994) 3338–3339.
[24] Y. Ichikawa, H. Kondo, Y. Igarashi, K. Noguchi, K. Okuyama, J. Washiyama, Crystal structures of α and β forms of poly (tetramethylene succinate), Polymer 41 (2000) 4719–4727.
[25] G.Z. Papageorgiou, D.S. Achilias, D.N. Bikiaris, Crystallization kinetics of biodegradable poly (butylene succinate) under isothermal and non-isothermal conditions, Macromol. Chem. Phys. 208 (2007) 1250–1264.
[26] Q. Yu, A. Anuar, A. Petzold, J. Balko, K. Saalwächter, T. Thurn-Albrecht, The semicrystalline morphology of polybutylene succinate supports a general scheme based on intracrystalline dynamics, Macromol. Chem. Phys. 224 (2023), 2200459.
[27] J.W. Park, D.K. Kim, S.S. Im, Crystallization behaviour of poly (butylene succinate) copolymers, Polym. Int. 51 (2002) 239–244.
[28] C. Schick, A. Toda, R. Androsch, The narrow thickness distribution of lamellae of poly (butylene succinate) formed at low melt supercooling, Macromolecules 54 (2021) 3366–3376.
[29] B. Wunderlich, The melting of defect polymer crystals, Polymer 5 (1964) 611–624.
[30] Y. Lee, R.S. Porter, J.S. Lin, On the double-melting behavior of poly (ether ether ketone), Macromolecules 22 (1989) 1756–1760.
[31] A. Toda, R. Androsch, C. Schick, Insights into polymer crystallization and melting from fast scanning chip calorimetry, Polymer 91 (2016) 239–263.
[32] M.C. Righetti, M.L. Di Lorenzo, D. Cavallo, A.J. Müller, M. Gazzano, Structural evolution of poly (butylene succinate) crystals on heating with the formation of a dual lamellar population, as monitored by temperature-dependent WAXS/SAXS analysis, Polymer 268 (2023), 125711.
[33] T. Fujimaki, Processability and properties of aliphatic polyesters, 'BIONOLLE', synthesized by polycondensation reaction, Polym. Degrad. Stabil. 59 (1998) 209–214.
[34] Y. Ichikawa, T. Mizukoshi, Bionolle (polybutylenesuccinate), Adv. Polym. Sci. 245 (2012) 285–313.
[35] H. Janeschitz-Kriegl, Crystallization Modalities in Polymer Melt Processing, Springer International Publishing, 2018.
[36] J.M. Haudin, N. Billon, Solidification of semi-crystalline polymers during melt processing, in: J.F. Janssson, U.W. Gedde (Eds.), Solidification Processes in Polymers, 132–137, Steinkopff, 1992.
[37] J.E.K. Schawe, Influence of processing conditions on polymer crystallization measured by fast scanning DSC, J. Therm. Anal. Calorim. 116 (2014) 1165–1173.
[38] K. Jariyavidyanont, J.L. Williams, A.M. Rhoades, I. Kühnert, W. Focke, R. Androsch, Crystallization of polyamide 11 during injection molding, Polym. Eng. Sci. 58 (2018) 1053–1061.
[39] C. Schick, R. Androsch, Nucleation-controlled semicrystalline morphology of bulk polymers, Polym. Cryst. 1 (2018), e10036.
[40] R. Androsch, M.L. Di Lorenzo, C. Schick, Optical microscopy to study crystal nucleation in polymers using a fast scanning chip calorimeter for precise control of the nucleation pathway, Macromol. Chem. Phys. 219 (2018), 1700479.
[41] Q. Zia, R. Androsch, H.-J. Radusch, E. Ingoliç, Crystal morphology of rapidly cooled isotactic polypropylene: a comparative study by TEM and AFM, Polym. Bull. 60 (2008) 791–798.
[42] T. Yamamoto, Molecular dynamics simulations of polymer crystallization in highly supercooled melt: primary nucleation and cold crystallization, J. Chem. Phys. 133 (2010), 034904.
[43] C. Schick, R. Androsch, J.W.P. Schmelzer, Homogeneous crystal nucleation in polymers, J. Phys. Condens. Matter 29 (2017), 453002.
[44] H.W. Starkweather Jr., R.E. Brooks, Effect of spherulites on the mechanical properties of nylon 66, J. Appl. Polym. Sci. 1 (1959) 236–239.
[45] W.G. Perkins, Polymer toughness and impact resistance, Polym. Eng. Sci. 39 (1999) 2445–2460.
[46] Q. Zia, R. Androsch, H.-J. Radusch, Effect of the structure at the micrometer and nanometer scales on the light transmission of isotactic polypropylene, J. Appl. Polym. Sci. 117 (2010) 1013–1020.
[47] D. Mileva, Q. Zia, R. Androsch, Tensile properties of random copolymers of propylene with ethylene and 1-butene: effect of crystallinity and crystal habit, Polym. Bull. 65 (2010) 623–634.
[48] R. Androsch, E. Zhuravlev, J.W.P. Schmelzer, C. Schick, Relaxation and crystal nucleation in polymer glasses, Eur. Polym. J. 102 (2018) 195–208.
[49] D.G. Papageorgiou, E. Zhuravlev, G.Z. Papageorgiou, D. Bikiaris, K. Chrissafis, C. Schick, Kinetics of nucleation and crystallization in poly (butylene succinate) nanocomposites, Polymer 55 (2014) 6725–6734.
[50] R. Zhang, K. Jariyavidyanont, E. Zhuravlev, C. Schick, R. Androsch, Zero-entropy-production melting temperature of crystals of poly (butylene succinate) formed at high supercooling of the melt, Macromolecules 55 (2022) 965–970.
[51] X. Wang, J. Zhou, L. Li, Multiple melting behavior of poly (butylene succinate), Eur. Polym. J. 43 (2007) 3163–3170.
[52] H. Suzuki, J. Grebowicz, B. Wunderlich, Glass transition of poly (oxymethylene), Br. Polym. J. 17 (1985) 1–3.
[53] B. Wunderlich, Reversible crystallization and the rigid–amorphous phase in semicrystalline macromolecules, Prog. Polym. Sci. 28 (2003) 383–450.
[54] L. Aliotta, M. Seggiani, A. Lazzeri, V. Gigante, P. Cinelli, A brief review of poly (butylene succinate) (PBS) and its main copolymers: synthesis, blends, composites, biodegradability, and applications, Polymers 14 (2022) 844.
[55] S. Charlon, L. Delbreilh, E. Dargent, N. Follain, J. Soulestin, S. Marais, Influence of crystallinity on the dielectric relaxations of poly (butylene succinate) and poly [(butylene succinate)-co-(butylene adipate)], Eur. Polym. J. 84 (2016) 366–376.
[56] S.F. Yao, X.T. Chen, H.M. Ye, Investigation of structure and crystallization behavior of poly (butylene succinate) by fourier transform infrared spectroscopy, J. Phys. Chem. B 121 (2017) 9476–9485.
[57] M.C. Righetti, M.L. Di Lorenzo, P. Cinelli, M. Gazzano, Temperature dependence of the rigid amorphous fraction of poly (butylene succinate), RSC Adv. 11 (2021) 25731–25737.
[58] C. Schick, R. Androsch, The origin of annealing peaks in semicrystalline polymers: enthalpy recovery or melting? Macromolecules 53 (2020) 8751–8756.
[59] Z.G. Wang, B.S. Hsiao, B.B. Sauer, W.G. Kampert, The nature of secondary crystallization in poly (ethylene terephthalate), Polymer 40 (1999) 4615–4627.
[60] R. Verma, H. Marand, B. Hsiao, Morphological changes during secondary crystallization and subsequent melting in poly (ether ether ketone) as studied by real time small angle X-ray scattering, Macromolecules 29 (1996) 7767–7775.
[61] G.R. Strobl, T. Engelke, H. Meier, G. Urban, H.G. Zachmann, R. Hosemann, V. Mathot, Zum Mechanismus der Polymerkristallisation, Colloid Polym. Sci. 260 (1982) 394–403.
[62] C.C. Hsu, P.H. Geil, H. Miyaji, K. Asai, Structure and properties of polypropylene crystallized from the glassy state, J. Polym. Sci. Polym. Phys. 24 (1986) 2379–2401.
[63] T. Ogawa, H. Miyaji, K. Asai, Nodular structure of polypropylene, J. Phys. Soc. Jpn. 54 (1985) 3668–3670.
[64] Q. Zia, R. Androsch, H.-J. Radusch, S. Piccarolo, Morphology, reorganization and stability of mesomorphic nanocrystals in isotactic polypropylene, Polymer 47 (2006) 8163–8172.
[65] D. Mileva, I. Kolesov, R. Androsch, Morphology of cold-crystallized polyamide 6, Colloid Polym. Sci. 290 (2012) 971–978.
[66] A.M. Gohn, A.M. Rhoades, N. Wonderling, T. Tighe, R. Androsch, The effect of supercooling of the melt on the semicrystalline morphology of PA 66, Thermochim. Acta 655 (2017) 313–318.
[67] A. Mollova, R. Androsch, D. Mileva, C. Schick, A. Benhamida, Effect of supercooling on crystallization of polyamide 11, Macromolecules 46 (2013) 828–835.
[68] J. Zhang, K. Tashiro, A.J. Domb, H. Tsuji, Confirmation of disorder α form of poly (L-lactic acid) by the X-ray fiber pattern and polarized IR/Raman spectra measured for uniaxially-oriented samples, Macromol. Symp. 242 (2006) 274–278.
[69] K. Wasanasuk, K. Tashiro, Crystal structure and disorder in poly(L-lactic acid) δ form (α′ form) and the phase transition mechanism to the ordered α form, Polymer 52 (2011) 6097–6109.
[70] G. Natta, P. Corradini, Structure and properties of isotactic polypropylene, Il Nuovo Cimento 15 (1960) 40–51.
[71] R. Androsch, M.L. Di Lorenzo, C. Schick, B. Wunderlich, Mesophases in polyethylene, polypropylene, and poly (1-butene), Polymer 51 (2010) 4639–4662.
[72] A. Ziabicki, Über die mesomorphe β-Form von Polycapronamid und ihre Umwandlung in die kristalline Form α, Kolloid-Zeitschr. 167 (1959) 132–141.
[73] A.M. Rhoades, N. Wonderling, C. Schick, R. Androsch, Supercooling-controlled heterogeneous and homogenous crystal nucleation of polyamide 11 and its effect onto the crystal/mesophase polymorphism, Polymer 106 (2016) 29–34.
[74] K. Jariyavidyanont, R. Zhang, Q. Yu, A. Janke, T. Thurn-Albrecht, C. Schick, R. Androsch, Formation of imperfect crystals in poly (ε-caprolactone) at high melt-supercooling, Mater. Lett. 324 (2022), 132704.
[75] C. Schick, V. Mathot, Fast Scanning Calorimetry, Springer, Cham, 2016.

[76] D. Baeten, D. Cavallo, G. Portale, R. Androsch, V. Mathot, B. Goderis, Combining fast scanning chip calorimetry with structural and morphological characterization techniques, in: C. Schick, V. Mathot (Eds.), Fast Scanning Calorimetry, Springer, Cham, 2016, pp. 327–359.
[77] M. van Drongelen, T. Meijer-Vissers, D. Cavallo, G. Portale, G. vanden Poel, R. Androsch, Microfocus wide-angle X-ray scattering of polymers crystallized in a fast scanning chip calorimeter, Thermochim. Acta 563 (2013) 33–37.
[78] D. Mileva, R. Androsch, E. Zhuravlev, C. Schick, Morphology of mesophase and crystals of polyamide 6 prepared in a fast scanning chip calorimeter, Polymer 53 (2012) 3994–4001.
[79] Product information MCPP Germany GmbH; https://www.mcpp-global.com/en/mcpp-english-europe/products/product/biopbsTM-general-properties/ (assessed 16/May/2022).
[80] Personal Communication with MCPP Germany GmbH, July/2019.
[81] K. Jariyavidyanont, A. Abdelaziz, R. Androsch, C. Schick, Experimental analysis of lateral thermal inhomogeneity of a specific chip-calorimeter sensor, Thermochim. Acta 674 (2019) 95–99.
[82] J.E.K. Schawe, S. Pogatscher, Material characterization by fast scanning calorimetry: practice and applications, in: C. Schick, V. Mathot (Eds.), Fast Scanning Calorimetry, 80, Springer, Cham, 2016, p. 3.
[83] M. Schulz, A. Seidlitz, R. Kurz, R. Baerenwald, A. Petzold, K. Saalwaechter, T. Thurn-Albrecht, The underestimated effect of intracrystalline chain dynamics on the morphology and stability of semicrystalline polymers, Macromolecules 51 (2018) 8377–8385.
[84] A. Seidlitz, T. Thurn-Albrecht, in: Q. Guo (Ed.), Polymer Morphology, 164, Wiley, Hoboken, NJ, USA, 2016, p. 151.
[85] W. Ruland, The evaluation of the small-angle scattering of lamellar two-phase systems by means of interface distribution functions, Colloid Polym. Sci. 255 (1977) 417–427.
[86] E. Turska, S. Gogolewski, Study on crystallization of nylon-6 (polycapramide): Part 2. Effect of molecular weight on isothermal crystallization kinetics, Polymer 12 (1971) 629–641.
[87] M.L. Di Lorenzo, P. Rubino, B. Immirzi, R. Luijkx, M. Hélou, R. Androsch, Influence of chain structure on crystal polymorphism of poly (lactic acid). Part 2. Effect of molecular mass on the crystal growth rate and semicrystalline morphology, Colloid Polym. Sci. 293 (2015) 2459–2467.
[88] M.L. Di Lorenzo, R. Androsch, Crystallization of poly [(R)-3-hydroxybutyrate], Adv. Polym. Sci. 283 (2019) 119–142.
[89] R. Androsch, C. Schick, Crystal nucleation of polymers at high supercooling of the melt, Adv. Polym. Sci. 276 (2015) 257–288.
[90] E. Zhuravlev, J.W.P. Schmelzer, B. Wunderlich, C. Schick, Kinetics of nucleation and crystallization in poly (ε-caprolactone) (PCL), Polymer 52 (2011) 1983–1997.
[91] A. Wurm, A. Herrmann, M. Cornelius, E. Zhuravlev, D. Pospiech, R. Nicula, C. Schick, Temperature dependency of nucleation efficiency of carbon nanotubes in PET and PBT, Macromol. Mater. Eng. 300 (2015) 637–649.
[92] R. Androsch, C. Schick, A.M. Rhoades, Application of Tammann's two-stage crystal nuclei development method for analysis of the thermal stability of homogeneous crystal nuclei of poly (ethylene terephthalate), Macromolecules 48 (2015) 8082–8089.
[93] J.D. Hoffman, J.I. Lauritzen Jr., Crystallization of bulk polymers with chain folding: theory of growth of lamellar spherulites, J. Res. Nat. Bur. Stand. Section A, Phys. Chem. 65 (1961) 297–336.
[94] M. Safari, A. Mugica, M. Zubitur, A. Martínez de Ilarduya, S. Muñoz-Guerra, A. J. Müller, Controlling the isothermal crystallization of isodimorphic PBS-ran-PCL random copolymers by varying composition and supercooling, Polymers 12 (2019) 17.
[95] G. Tammann, Ueber die Abhängigkeit der Zahl der Kerne, welche sich in verschiedenen unterkühlten Flüssigkeiten bilden, von der Temperatur, Zeitschr. f. Phys. Chem. 25 (1898) 441–479.
[96] K. Jariyavidyanont, E. Zhuravlev, C. Schick, R. Androsch, Kinetics of homogeneous crystal nucleation of polyamide 11 near the glass transition temperature, Polym. Cryst. 4 (2021), e10149.
[97] E. Zhuravlev, A. Wurm, P. Pötschke, R. Androsch, J.W.P. Schmelzer, C. Schick, Kinetics of nucleation and crystallization of poly (ε-caprolactone)–multiwalled carbon nanotube composites, Eur. Polym. J. 52 (2014) 1–11.
[98] E. Zhuravlev, J.W.P. Schmelzer, A.S. Abyzov, V.M. Fokin, R. Androsch, C. Schick, Experimental test of Tammann's nuclei development approach in crystallization of macromolecules, Cryst. Growth Des. 15 (2015) 786–798.
[99] S. Quattrosoldi, N. Lotti, M. Soccio, C. Schick, R. Androsch, Stability of crystal nuclei of poly (butylene isophthalate) formed near the glass transition temperature, Polymers 12 (2020) 1099.
[100] R.A. Andrianov, R. Androsch, R. Zhang, T.A. Mukhametzyanov, A. Abyzov, J.W. P. Schmelzer, C. Schick, Growth and dissolution of crystal nuclei in poly(ι-lactic acid) (PLLA) in Tammann's development method, Polymer 196 (2020), 122453.
[101] R.A. Andrianov, J.W.P. Schmelzer, R. Androsch, T.A. Mukhametzyanov, C. Schick, Radial growth rate of near-critical crystal nuclei in poly(ι-lactic acid) (PLLA) in Tammann's two-stage development method, J. Chem. Phys. 158 (2023), 054504.
[102] J. Deubener, M. Montazerian, S. Krüger, O. Peitl, E.D. Zanotto, Heating rate effects in time-dependent homogeneous nucleation in glasses, J. Non-Cryst. Sol. 474 (2017) 1–8.
[103] F. De Santis, R. Pantani, G. Titomanlio, Nucleation and crystallization kinetics of poly (lactic acid), Thermochim. Acta 522 (2011) 128–134.
[104] R. Androsch, C. Schick, J.W.P. Schmelzer, Sequence of enthalpy relaxation, homogeneous crystal nucleation and crystal growth in glassy polyamide 6, Eur. Polym. J. 53 (2014) 100–108.
[105] J. Xu, B.H. Guo, Microbial succinic acid, its polymer poly (butylene succinate), and applications, in: G.Q. Chen (Ed.), Plastics from Bacteria: Natural Functions and Applications, vol. 14, Springer, Berlin, 2010, pp. 347–388.
[106] T. Wang, H. Wang, H. Li, Z. Gan, S. Yan, Banded spherulitic structures of poly (ethylene adipate), poly (butylene succinate) and in their blends, Phys. Chem. Chem. Phys. 11 (2009) 1619–1627.
[107] T.X. Jin, M. Zhou, S.D. Hu, F. Chen, Q. Fu, Y. Fu, Effect of molecular weight on the properties of poly (butylene succinate), Chin. J. Polym. Sci. 32 (2014) 953–960.
[108] T. Yarici, M. Kodal, G. Ozkoc, Non-isothermal crystallization kinetics of poly (butylene succinate) (PBS) nanocomposites with different modified carbon nanotubes, Polymer 146 (2018) 361–377.
[109] K. Cho, J. Lee, K. Kwon, Hydrolytic degradation behavior of poly (butylene succinate) s with different crystalline morphologies, J. Appl. Polym. Sci. 79 (2001) 1025–1033.
[110] D. Mileva, Q. Zia, R. Androsch, H.J. Radusch, S. Piccarolo, Mesophase formation in poly (propylene-ran-1-butene) by rapid cooling, Polymer 50 (2009) 5482–5489.
[111] R. Androsch, A.M. Rhoades, I. Stolte, C. Schick, Density of heterogeneous and homogeneous crystal nuclei in poly (butylene terephthalate), Eur. Polym. J. 66 (2015) 180–189.
[112] F. Rybnikář, Secondary crystallization of polymers, J. Polym. Sci. 44 (1960) 517–522.
[113] D.C. Bassett, R.H. Olley, I.A.M. Al Raheil, On crystallization phenomena in PEEK, Polymer 29 (1988) 1745–1754.
[114] F.P. Price, A phenomenological theory of spherulitic crystallization: primary and secondary crystallization processes, J. Polym. Sci. General Papers 3 (1965) 3079–3086.
[115] K. Mezghani, R. Anderson Campbell, P.J. Phillips, Lamellar thickening and the equilibrium melting point of polypropylene, Macromolecules 27 (1994) 997–1002.
[116] K. Kamide, K. Yamaguchi, Change in fine structures of isotactic polypropylene during isothermal crystallization, Makromol. Chem. Macromol. Chem. Phys. 162 (1972) 219–233.
[117] P. Maiti, M. Hikosaka, K. Yamada, A. Toda, F. Gu, Lamellar thickening in isotactic polypropylene with high tacticity crystallized at high temperature, Macromolecules 33 (2000) 9069–9075.
[118] J.M. Schultz, R.D. Scott, Temperature dependence of secondary crystallization in linear polyethylene, J. Polym. Sci. Polym. Phys. 7 (1969) 659–666.
[119] A. Alizadeh, L. Richardson, J. Xu, S. McCartney, H. Marand, Y.W. Cheung, S. Chum, Influence of structural and topological constraints on the crystallization and melting behavior of polymers. 1. Ethylene/1-octene copolymers, Macromolecules 32 (1999) 6221–6235.
[120] B.S. Hsiao, B.B. Sauer, R.K. Verma, H.G. Zachmann, S. Seifert, B. Chu, P. Harney, New insight of isothermal melt crystallization in poly (aryl ether ether ketone) via time-resolved simultaneous small-angle X-ray scattering/wide-angle X-ray diffraction measurements, Macromolecules 28 (1995) 6931–6936.
[121] Z. Qiu, S. Fujinami, M. Komura, K. Nakajima, T. Ikehara, T. Nishi, Nonisothermal crystallization kinetics of poly (butylene succinate) and poly (ethylene succinate), Polym. J. 36 (2004) 642–646.
[122] A.A. Minakov, D.A. Mordvintsev, C. Schick, Melting and reorganization of poly (ethylene terephthalate) on fast heating (1000 K/s), Polymer 45 (2004) 3755–3763.
[123] S. Charlon, S. Marais, E. Dargent, J. Soulestin, M. Sclavons, N. Follain, Structure–barrier property relationship of biodegradable poly (butylene succinate) and poly [(butylene succinate)-co-(butylene adipate)] nanocomposites: influence of the rigid amorphous fraction, Phys. Chem. Chem. Phys. 17 (2015) 29918–29934.
[124] E.W. Fischer, G.F. Schmidt, Long periods in drawn polyethylene, Angew. Chem., Int. Ed. 1 (1962) 488–499.
[125] F. Rybnikář, Mechanism of secondary crystallization in polymers, J. Polym. Sci. Part A 1 (1963) 2031–2038.
[126] A. Peterlin, Crystallization and annealing of polyethylene, Makromol. Chem.: Macromol. Chem. Phys. 74 (1964) 107–128.
[127] M. Gordon, I.H. Hillier, Mechanism of secondary crystallization of polymethylene, Phil. Mag. 11 (1965) 31–41.
[128] J.N. Hay, Secondary crystallization kinetics, Polym. Cryst. 1 (2018), e10007.
[129] E. Hellmuth, B. Wunderlich, Superheating of linear high-polymer polyethylene crystals, J. Appl. Phys. 36 (1965) 3039–3044.
[130] D.R. Lippits, S. Rastogi, G.W.H. Höhne, Melting kinetics in polymers, Phys. Rev. Lett. 96 (2006), 218303.
[131] A. Toda, M. Hikosaka, K. Yamada, Superheating of the melting kinetics in polymer crystals: a possible nucleation mechanism, Polymer 43 (2002) 1667–1679.
[132] A. Toda, R. Androsch, C. Schick, Melting kinetics of superheated polymer crystals examined by isothermal and nonisothermal fast scanning calorimetry, Macromolecules 54 (2021) 8770–8779.
[133] S. Van Herwaarden, E. Iervolino, F. Van Herwaarden, T. Wijffels, A. Leenaers, V. Mathot, Design, performance and analysis of thermal lag of the UFS1 twin-calorimeter chip for fast scanning calorimetry using the Mettler-Toledo Flash DSC 1, Thermochim. Acta 522 (2011) 46–52.
[134] J.E.K. Schawe, Measurement of the thermal glass transition of polystyrene in a cooling rate range of more than six decades, Thermochim. Acta 603 (2015) 128–134.

[135] J.E.K. Schawe, Temperature correction at high heating rates for conventional and fast differential scanning calorimetry, Thermochim. Acta 698 (2021), 178879.
[136] J.D. Hoffman, G.T. Davis, J.I. Lauritzen Jr., The rate of crystallization of linear polymers with chain folding, in: N.B. Hannay (Ed.), Treatise on Solid State Chemistry: Volume 3 Crystalline and Noncrystalline Solids, Springer, Boston, 1976, pp. 497–614.
[137] B. Wunderlich, Macromolecular Physics, vol. 3, Academic Press, New York, 1980. *Crystal Melting*.
[138] J.D. Hoffman, J.J. Weeks, Melting process and the equilibrium melting temperature of polychlorotrifluoroethylene, J. Res. Natl. Bur. Stand. Sect. A 66 (1962) 13–28.
[139] K. Yamada, M. Hikosaka, A. Toda, S. Yamazaki, K. Tagashira, Equilibrium melting temperature of isotactic polypropylene with high tacticity: 1. Determination by differential scanning calorimetry, Macromolecules 36 (2003) 4790–4801.
[140] P. Pan, B. Zhu, W. Kai, T. Dong, Y. Inoue, Polymorphic transition in disordered poly (l-lactide) crystals induced by annealing at elevated temperatures, Macromolecules 41 (2008) 4296–4304.
[141] J. Zhang, K. Tashiro, H. Tsuji, A.J. Domb, Disorder-to-order phase transition and multiple melting behavior of poly (l-lactide) investigated by simultaneous measurements of WAXD and DSC, Macromolecules 41 (2008) 1352–1357.
[142] R. Lv, Y. He, J. Wang, J. Wang, J. Hu, J. Zhang, W. Hu, Flash DSC study on the annealing behaviors of poly (l-lactide acid) crystallized in the low temperature region, Polymer 174 (2019) 123–129.
[143] K. Jariyavidyanont, M. Du, Q. Yu, T. Thurn-Albrecht, C. Schick, R. Androsch, Bulk enthalpy of melting of poly(L-lactic acid) (PLLA) determined by fast scanning chip calorimetry, Macromol. Rapid Commun. 43 (2022), 2200148.
[144] K. Jariyavidyanont, C. Schick, R. Androsch, The bulk enthalpy of melting of α'-crystals of poly(L-lactic acid) determined by fast scanning chip calorimetry, Thermochim. Acta 717 (2022), 179349.
[145] G.Z. Papageorgiou, D.G. Papageorgiou, K. Chrissafis, D. Bikiaris, J. Will, A. Hoppe, J.A. Roether, A.R. Boccaccini, Crystallization and melting behavior of poly (butylene succinate) nanocomposites containing silica-nanotubes and strontium hydroxyapatite nanorods, Ind. Eng. Chem. Res. 53 (2014) 678–692.
[146] Z. Qiu, W. Yang, Crystallization kinetics and morphology of poly (butylene succinate)/poly (vinyl phenol) blend, Polymer 47 (2006) 6429–6437.
[147] M. Kakudo, N. Kasai, X-Ray Diffraction by Polymers, Kodansha Ltd., Tokyo, 1972.
[148] J. Zhang, Y. Duan, H. Sato, H. Tsuji, I. Noda, S. Yan, Y. Ozaki, Crystal modifications and thermal behavior of poly(L-lactic acid) revealed by infrared spectroscopy, Macromolecules 38 (2005) 8012–8021.
[149] J. Runt, M. Kanchanasopa, Crystallinity determination, in: Encyclopedia of Polymer Science and Technology, Wiley, 2002.
[150] I. Arandia, N. Zaldua, J. Maiz, R.A. Pérez-Camargo, A. Mugica, M. Zubitur, R. Mincheva, P. Dubois, A.J. Müller, Tailoring the isothermal crystallization kinetics of isodimorphic poly (butylene succinate-ran-butylene azelate) random copolymers by changing composition, Polymer 183 (2019), 121863.
[151] J.M. Schultz, J.S. Lin, R.W. Hendricks, A dynamic study of the crystallization of polyethylene from the melt, J. Appl. Crystallogr. 11 (1978) 551–557.
[152] Y. Tanabe, G.R. Strobl, E.W. Fischer, Surface melting in melt-crystallized linear polyethylene, Polymer 27 (1986) 1147–1153.
[153] M. Schulz, M. Schäfer, K. Saalwächter, T. Thurn-Albrecht, Competition between crystal growth and intracrystalline chain diffusion determines the lamellar thickness in semicrystalline polymers, Nat. Commun. 13 (2022) 119.
[154] J.P. Kalish, K. Aou, X. Yang, S.L. Hsu, Spectroscopic and thermal analyses of α′ and α crystalline forms of poly(L-lactic acid), Polymer 52 (2011) 814–821.
[155] M.C. Righetti, M. Gazzano, M.L. Di Lorenzo, R. Androsch, Enthalpy of melting of α′-and α-crystals of poly(L-lactic acid), Eur. Polym. J. 70 (2015) 215–220.
[156] H. Xu, B.S. Ince, P. Cebe, Development of the crystallinity and rigid amorphous fraction in cold-crystallized isotactic polystyrene, J. Polym. Sci. Polym. Phys. 41 (2003) 3026–3036.
[157] M.C. Righetti, M.L. Di Lorenzo, E. Tombari, M. Angiuli, The low-temperature endotherm in poly (ethylene terephthalate): partial melting and rigid amorphous fraction mobilization, J. Phys. Chem. B 112 (2008) 4233–4241.
[158] M.L. Di Lorenzo, M. Gazzano, M.C. Righetti, The role of the rigid amorphous fraction on cold crystallization of poly (3-hydroxybutyrate), Macromolecules 4 (2012) 5684–5691.
[159] J. Martín, N. Stingelin, D. Cangialosi, Direct calorimetric observation of the rigid amorphous fraction in a semiconducting polymer, J. Phys. Chem. Lett. 9 (2018) 990–995.
[160] M.C. Righetti, P. Marchese, M. Vannini, A. Celli, C. Lorenzetti, D. Cavallo, C. Ocando, A.J. Müller, R. Androsch, Polymorphism and multiple melting behavior of bio-based poly (propylene 2, 5-furandicarboxylate), Biomacromolecules 21 (2020) 2622–2634.
[161] Z. Wei, Y. Yu, C. Zhou, L. Zheng, X. Leng, Y. Li, Relationship between melting behavior and morphological changes of semicrystalline polymers: evidence from the case of poly (hexamethylene succinate), J. Therm. Anal. Calorim. 129 (2017) 777–787.
[162] B. Wunderlich, H. Baur, Heat capacities of linear high polymers, Adv. Polym. Sci. 7 (1970) 151–368.
[163] B. Wunderlich, Study of the change in specific heat of monomeric and polymeric glasses during the glass transition, J. Phys. Chem. 64 (1960) 1052–1056.
[164] S. Quattrosoldi, R. Androsch, A. Janke, M. Soccio, N. Lotti, Enthalpy relaxation, crystal nucleation and crystal growth of biobased poly (butylene isophthalate), Polymers 12 (2020) 235.